

Electronic Thesis and Dissertation Repository

8-10-2017 12:00 AM

Hydrodynamics in the Gas-Driven Inverse Liquid-Solid Fluidized Bed

Jiaqi Huang, *The University of Western Ontario*

Supervisor: Jesse Zhu, *The University of Western Ontario*

A thesis submitted in partial fulfillment of the requirements for the Master of Engineering Science degree in Chemical and Biochemical Engineering

© Jiaqi Huang 2017

Follow this and additional works at: <https://ir.lib.uwo.ca/etd>

 Part of the [Catalysis and Reaction Engineering Commons](#), and the [Other Chemical Engineering Commons](#)

Recommended Citation

Huang, Jiaqi, "Hydrodynamics in the Gas-Driven Inverse Liquid-Solid Fluidized Bed" (2017). *Electronic Thesis and Dissertation Repository*. 4755.
<https://ir.lib.uwo.ca/etd/4755>

This Dissertation/Thesis is brought to you for free and open access by Scholarship@Western. It has been accepted for inclusion in Electronic Thesis and Dissertation Repository by an authorized administrator of Scholarship@Western. For more information, please contact wlsadmin@uwo.ca.

Abstract

A novel reactor named Gas-Driven Inverse Liquid-Solid Fluidized Bed (GDFB for short) was developed in this research. A vertical baffle divides the column into a riser and a downer. Inverse fluidization is driven by the gas and occurs in the downer, where hydrodynamics and their influencing factors were studied. In the solid-baffle system, four fluidization regimes were observed, including the packed bed, semi-fluidized bed, fully-fluidized bed, and circulating bed. Bed expansion ratio was higher for particles with a higher density and a smaller solids loading. Moreover, the average particle velocity was proportional to superficial gas velocity and higher for denser particles. In the meshed-baffle system, the shifted bed was found between the fully-fluidized bed and the circulating bed, and some hydrodynamics differed from that in the solid-baffle system. Considering the similarity and diversity, a solid baffle or a meshed baffle should be selected depending on the needs of chemical processes.

Keywords

Inverse Liquid-Solid Fluidized Bed (ILSFB), inverse fluidization, fluidization regime, gas velocity, solids loading, bed expansion, particle properties, particle circulation, particle velocity

Co-Authorship Statement

Title: Hydrodynamics in the Gas-Driven Inverse Liquid-Solid Fluidized Bed

Author: Jiaqi Huang, Jesse Zhu

The experimental apparatus of the Gas-Driven Inverse Liquid-Solid Fluidized Bed (GDILSFB) was constructed by Jiaqi Huang under the guidance of Dr. Jesse Zhu. Jiaqi Huang performed all the experiments and wrote the drafts of this manuscript. Data analysis and modifications of this work were undertaken with the advice from Dr. Jesse Zhu. The final version of this paper is ready for submission.

Title: Gas-Driven Inverse Liquid-Solid Fluidized Bed with Circulation

Author: Jiaqi Huang, Jesse Zhu, Tian Nan

The experimental apparatus of the Gas-Driven Inverse Liquid-Solid Fluidized Bed (GDILSFB) was constructed and modified by Jiaqi Huang under the guidance of Dr. Jesse Zhu and assisted by Tian Nan. Jiaqi Huang performed all the experiments and wrote the drafts of this manuscript. Data analysis and modifications of this work were undertaken with the advice from Dr. Jesse Zhu and Tian Nan. The final version of this paper is ready for submission.

Acknowledgments

I would like to take this chance to express the appreciation and gratitude to all those who have been supporting me in the academic and daily life.

My sincerest gratitude is expressed to Professor Jesse Zhu for being my supervisor, and especially for giving me the opportunity to start my Master's study. Thanks to his instructions and motivation, I was able to complete my research project and learn practical problem-solving skills in the meanwhile. His achievement and personality will continuously encourage me to pursue further self-improvement for the rest of my life.

I would like to express my deepest appreciation to Tian Nan for his guidance and help throughout the entire study. He is always an excellent colleague and a reliable friend.

My gratefulness is also directed to all my friends in the research group for their help in the academic and daily life. Special thanks go to Xiaoyang Wei for his guidance and advice in data analysis.

Much appreciation is extended to George Zhang for his technical support in the laboratory.

Finally, I would like to thank my family, especially my parents, for their unconditional support, encouragement, and love. Without them, I could not have accomplished my graduate study.

Table of Contents

Abstract.....	i
Co-Authorship Statement.....	ii
Acknowledgments.....	iii
Table of Contents.....	iv
List of Tables.....	vii
List of Figures.....	viii
List of Appendices.....	xi
Chapter 1.....	1
1 General Introduction.....	1
1.1 Introduction.....	1
1.2 Objectives.....	3
1.3 Thesis Structures.....	3
References.....	4
Chapter 2.....	6
2 Hydrodynamics in the Gas-Driven Inverse Liquid-Solid Fluidized Bed.....	6
2.1 Introduction.....	6
2.2 Experimental Apparatus and Procedures.....	8
2.3 The Main System.....	12
2.3.1 The Inverse Fluidization Regimes.....	12
2.3.2 Initial and Uniform Fluidization Velocities.....	13
2.3.3 Bed Expansion.....	16
2.4 The Alternative System.....	27
2.4.1 The Inverse Fluidization Regimes.....	27
2.4.2 Initial and Uniform Fluidization Velocities.....	28

2.4.3	Bed Expansion	30
2.5	Conclusions.....	33
	Nomenclature	34
	References	36
Chapter 3.....		38
3	Gas-Driven Inverse Liquid-Solid Fluidized Bed with Circulation	38
3.1	Introduction.....	38
3.2	Materials and Methods.....	40
3.2.1	Experimental Apparatus and Procedures	40
3.2.2	Optical Fiber Probe (OFP)	44
3.3	The Main System	45
3.3.1	The Fluidization Regimes	45
3.3.2	Transition Velocity	47
3.3.3	Average Particle Velocity	48
3.4	The Alternative System.....	53
3.4.1	The Fluidization Regimes	53
3.4.2	Transition Velocity	54
3.4.3	Average Particle Velocity	55
3.5	Conclusions.....	57
	Nomenclature	58
	References	60
Chapter 4.....		63
4	Conclusions and Recommendations	63
4.1	Conclusions.....	63
4.2	Recommendations.....	64

Appendices.....	65
Appendix A. Examples of error analysis	65
Appendix B1. Initial fluidization velocity, uniform fluidization velocity, and transition velocity.....	67
Appendix B2. Average particle velocity	68
Appendix C. Rotameter calibration.....	70
Curriculum Vitae	71

List of Tables

<i>Table 2.1 List of particles and their properties</i>	10
<i>Table 2.2 Summary of linear relationship between the logarithms of bed expansion ratio ($\log_{10}(H/H_0)$) (y) and excess superficial gas velocity ($U_G - U_{if}$) (x)</i>	25
<i>Table 3.1 List of particles and their properties</i>	42
<i>Table 3.2 Linear equations for predicting the average particle velocity (y) based on the superficial gas velocity (x)</i>	49

List of Figures

<i>Figure 1.1 Sketch of the GDFB</i>	2
<i>Figure 2.1 Simplified schematic diagram of the GDFB</i>	7
<i>Figure 2.2 Schematic diagram of the GDFB and the cross-sectional view of column</i>	9
<i>Figure 2.3 Photo of the particles used in the experiments</i>	10
<i>Figure 2.4 Enlarged mesh</i>	11
<i>Figure 2.5 The inverse fluidization regimes in the main system</i>	13
<i>Figure 2.6 Initial fluidization velocity (U_{if}) versus solids loading for three types of particles in the main system.</i>	14
<i>Figure 2.7 Uniform fluidization velocity (U_{uf}) versus solids loading for three types of particles in the main system.</i>	16
<i>Figure 2.8 Bed expansion ratio (H/H_0) against the excess superficial gas velocity ($U_G - U_{if}$) at different solids loadings for particles with a density of (a) 904 kg/m^3, (b) 930 kg/m^3, and (c) 950 kg/m^3 in the main system.</i>	19
<i>Figure 2.9 Fluidization ratio (H_f/H_0) against the excess superficial gas velocity ($U_G - U_{if}$) at different solids loadings for particles with a density of (a) 904 kg/m^3, (b) 930 kg/m^3, and (c) 950 kg/m^3 in the main system.</i>	21
<i>Figure 2.10 Fraction of packed bed (H_p/H) against the excess superficial gas velocity ($U_G - U_{if}$) at different solids loadings for particles with a density of (a) 904 kg/m^3, (b) 930 kg/m^3, and (c) 950 kg/m^3 in the main system.</i>	23
<i>Figure 2.11 Bed expansion ratio (H/H_0) against the excess superficial gas velocity ($U_G - U_{if}$) for three types of particles at (a) 5% solids loading and (b) 10% solids loading in the main system.</i>	24

<i>Figure 2.12 Logarithms of bed expansion ratio (H/H_0) against the excess superficial gas velocity ($U_G - U_{if}$) at 5%, 10%, and 15% solids loadings for particles with a density of (a) 904 kg/m^3 and (b) 930 kg/m^3 in the main system.</i>	<i>26</i>
<i>Figure 2.13 The inverse fluidization regimes in the alternative system</i>	<i>28</i>
<i>Figure 2.14 Initial fluidization velocity (U_{if}) versus solids loading for particles with a density of 930 kg/m^3 in the main system with solid baffle and in the alternative system with a meshed baffle.....</i>	<i>29</i>
<i>Figure 2.15 Uniform fluidization velocity (U_{uf}) versus solids loading for particles with a density of 930 kg/m^3 in the main system with solid baffle and in the alternative system with a meshed baffle.....</i>	<i>30</i>
<i>Figure 2.16 Bed expansion ratio (H/H_0) against the excess superficial gas velocity ($U_G - U_{if}$) at different solids loadings for particles with a density of 930 kg/m^3 in the alternative system.....</i>	<i>31</i>
<i>Figure 2.17 Fluidization ratio (H_f/H_0) against the excess superficial gas velocity ($U_G - U_{if}$) at different solids loadings for particles with 930 kg/m^3 in the alternative system. .</i>	<i>32</i>
<i>Figure 2.18 Fraction of packed bed (H_p/H) against excess superficial gas velocity ($U_G - U_{if}$) at different solids loadings for particles with 930 kg/m^3 in the alternative system. .</i>	<i>32</i>
<i>Figure 3.1 Sketch of the GDFB.....</i>	<i>39</i>
<i>Figure 3.2 Schematic drawing of the GDFB and the cross section of column.....</i>	<i>41</i>
<i>Figure 3.3 Photo of particles used in this study</i>	<i>42</i>
<i>Figure 3.4 Enlarged mesh.....</i>	<i>43</i>
<i>Figure 3.5 OFP diagram for particle velocity measurement (Sang, 2013).....</i>	<i>44</i>
<i>Figure 3.6 Cross-sectional view of the column with the radial position of the OFP</i>	<i>45</i>

<i>Figure 3.7 The fluidization regimes of the GDFB in the main system</i>	<i>46</i>
<i>Figure 3.8 Transition velocity (U_{tr}) against solids loading for three types of particles in the main system.</i>	<i>48</i>
<i>Figure 3.9 Average particle velocity (U_p) versus the superficial gas velocity (U_G) at different solids loadings for particles with a density of (a) 904 kg/m^3, (b) 930 kg/m^3, and (c) 950 kg/m^3 in the main system.</i>	<i>51</i>
<i>Figure 3.10 Average particle velocity (U_p) versus superficial gas velocity (U_G) for three types of particles at (a) 5% solids loading and (b) 10% solids loading in the main system.</i>	<i>52</i>
<i>Figure 3.11 The fluidization regimes of the GDFB in the alternative system</i>	<i>53</i>
<i>Figure 3.12 Transition velocity (U_{tr}) versus solids loading for particles with 930 kg/m^3 in the main system with a solid baffle and in the alternative system with a meshed baffle. .</i>	<i>54</i>
<i>Figure 3.13 Average particle velocity (U_p) versus superficial gas velocity (U_G) at different solids loadings for particles with 930 kg/m^3 in the alternative system.</i>	<i>55</i>
<i>Figure 3.14 Average particle velocity (U_p) versus superficial gas velocity (U_G) at 15% solids loading for particles with 930 kg/m^3 in the alternative system and the main system.</i>	<i>56</i>
<i>Figure. A Initial fluidization velocity (U_{if}) versus solids loading with error bars for particles with a density of 930 kg/m^3 in the main system and in the alternative system. .</i>	<i>65</i>
<i>Figure. B Bed expansion ratio (H/H_0) with error bars for particles with 904 kg/m^3 at 5% solids loading in the main system.</i>	<i>66</i>
<i>Figure. C Average particle velocity (U_p) versus superficial gas velocity (U_G) with error bars for particles with a density of 930 kg/m^3 at 15% solids loading in the main system.</i>	<i>66</i>

Figure. D Rotameter calibration curve 70

List of Appendices

Appendix A. Examples of error analysis 65

Appendix B1. Initial fluidization velocity, uniform fluidization velocity, and
transition velocity..... 67

Appendix B2. Average particle velocity 68

Appendix C. Rotameter calibration..... 70

Chapter 1

1 General Introduction

1.1 Introduction

The traditional fluidization applies to solid particles having a higher density than the fluid. When a gas or liquid flows opposite to the direction of the gravity and counters the net downward force of the particles, fluidization of particles is realized. In contrast, to fluidize light particles with a density lower than the liquid, the liquid stream must be flowing downward to overcome the net buoyancy force. Such a system is known as the inverse fluidization (Fan, Muroyama, & Chern, 1982). Inverse fluidized beds have attracted more and more attention in the past decades due to their advantages over the upward fluidized beds. For example, inverse fluidization contributes to the maintenance of high mass transfer rate and appropriate biofilm thickness (Nikolov & Karamanev, 1987), the efficient process control (Renganathan & Krishnaiah, 2004), and re-fluidization after breakdown (Renganathan & Krishnaiah, 2003). Thus, inverse fluidized beds have been employed in various biological processes, including ferrous iron oxidation, wastewater treatment (Nikolov & Karamanev, 1987), and phenol biodegradation (Sabarunisha Begum & Radha, 2014).

Moreover, compared to conventional fluidization, circulating fluidized beds are able to reduce the back-mixing of phases and increase the interfacial contact efficiency (Zhu et al., 2000). Hence, liquid-solid circulating fluidized beds (LSCFB) have been introduced to several industries, such as the continuous recovery of whey proteins (Lan et al., 2000), the enzymatic phenol polymerization (Trivedi, Bassi, & Zhu, 2006), and the extractive fermentation of lactic acid (Patel et al., 2008). Also, biological nutrients in the municipal wastewater could be removed by an LSCFB in the pilot scale (Chowdhury et al., 2009).

In this study, combining the benefits of inverse fluidized beds and circulating fluidization, the novel Gas-Driven Inverse Liquid-Solid Fluidized Bed (GDILSFB or GDFB for short) was developed. The significant difference between the GDFB and the common-known liquid-solid fluidized bed is that the driving force of fluidization is a gas

stream instead of a continuous liquid flow. *Figure 1.1* shows a sketch of the GDFB. The column consists of a riser and a downer separated by a baffle. The gas fed into the riser drives the inverse fluidization of light particles in the downer. When the gas flowrate is sufficient, particles can circulate around the baffle continuously. As a result, proper operating conditions, both conventional inverse fluidization and circulating fluidization can be achieved in the GDFB. A detailed description will be given in the later chapters. The goal of introducing this new reactor is to offer another option in biological processes which require high mass transfer rate and low energy consumption. Especially in wastewater treatment, the GDFB might be beneficial for the control of biofilm thickness and handling of large capacities.

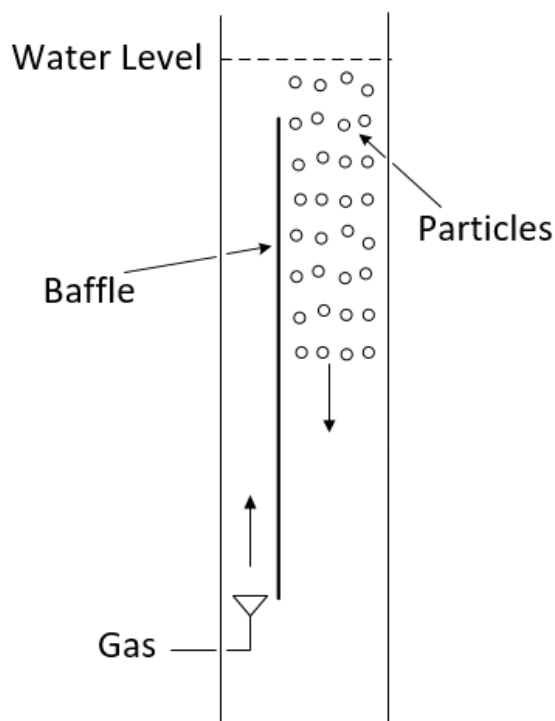


Figure 1.1 Sketch of the GDFB

1.2 Objectives

To understand the novel gas-driven inverse liquid-solid fluidized bed (GDFB) and explore its potential applications, the objectives of this research include:

1. Design and construct the GDFB and test the operating conditions for achieving fluidization.
2. Investigate some basic hydrodynamic characteristics of the GDFB, such as the fluidization regimes, bed expansion, and particle velocity.
3. Study the effects of particle properties, solids loading, superficial gas velocity, and baffle structure on the hydrodynamics.

1.3 Thesis Structures

This thesis contains four chapters and follows the integrated article format.

Chapter 1 provides a general introduction about the background and objectives of the current research as well as the thesis structure.

Chapter 2 reports the hydrodynamics in the GDFB, including the fluidization regimes, initial fluidization velocity, uniform fluidization velocity, and bed expansion. The influence of particle properties, solids loading, superficial gas velocity, and baffle structure are described as well.

Chapter 3 focuses on the circulation of particles in the GDFB. The transition velocity and average particle velocity are discussed along with the effects of superficial gas velocity, solids loading, particle properties, and baffle structure.

Chapter 4 gives the conclusions of this study and recommendations for future research.

References

- Chowdhury, N., Zhu, J., Nakhla, G., Patel, A., & Islam, M. (2009). A Novel Liquid-Solid Circulating Fluidized-Bed Bioreactor for Biological Nutrient Removal from Municipal Wastewater. *Chemical Engineering and Technology*, 32(3), 364–372. <http://doi.org/10.1002/ceat.200800564>
- Fan, L., Muroyama, K., & Chern, S.-H. (1982). Hydrodynamic Characteristics of Inverse Fluidization in Liquid-Solid and Gas-Liquid-Solid Systems. *The Chemical Engineering Journal*, 24, 143–150.
- Lan, Q., Zhu, J. (Jesse), Bassi, A. S., Margaritis, A., Zheng, Y., & Rowe, G. E. (2000). Continuous Protein Recovery Using a Liquid-Solid Circulating Fluidized Bed Ion Exchange System: Modelling and Experimental Studies. *The Canadian Journal of Chemical Engineering*, 78, 858–866.
- Nikolov, L., & Karamanov, D. (1987). Experimental Study of the Inverse Fluidized Bed Biofilm Reactor. *The Canadian Journal of Chemical Engineering*, 65(April 1987), 214–217.
- Patel, M., Bassi, A. S., Zhu, J. J.-X., & Goma, H. (2008). Investigation of a Dual-Particle Liquid-Solid Circulating Fluidized Bed Bioreactor for Extractive Fermentation of Lactic Acid. *Biotechnology Progress*, 24, 821–831. <http://doi.org/10.1021/bp.6>
- Renganathan, T., & Krishnaiah, K. (2003). Prediction of Minimum Fluidization Velocity in Two and Three Phase Inverse Fluidized Beds. *The Canadian Journal of Chemical Engineering*, 81(August), 853–860.
- Renganathan, T., & Krishnaiah, K. (2004). Liquid phase mixing in 2-phase liquid-solid inverse fluidized bed. *Chemical Engineering Journal*, 98(August 2003), 213–218. <http://doi.org/10.1016/j.cej.2003.08.001>
- Sabarunisha Begum, S., & Radha, K. V. (2014). Hydrodynamic behavior of inverse fluidized bed biofilm reactor for phenol biodegradation using *Pseudomonas*

fluorescens. *Korean Journal of Chemical Engineering*, 31(3), 436–445.
<http://doi.org/10.1007/s11814-013-0260-z>

Trivedi, U., Bassi, A., & Zhu, J.-X. (Jesse). (2006). Continuous enzymatic polymerization of phenol in a liquid-solid circulating fluidized bed. *Powder Technology*, 169, 61–70. <http://doi.org/10.1016/j.powtec.2006.08.001>

Zhu, J.-X. (Jesse), Zheng, Y., Karamanev, D. G., & Bassi, A. S. (2000). (Gas-) Liquid-Solid Circulating Fluidized Beds and their Potential Applications to Bioreactor Engineering. *The Canadian Journal of Chemical Engineering*, 78(February), 82–94.

Chapter 2

2 Hydrodynamics in the Gas-Driven Inverse Liquid-Solid Fluidized Bed

2.1 Introduction

In the classic fluidization, solid particles with a density higher than the fluid are fluidized by a liquid or gas stream flowing in the opposite direction to that of gravity. When the particles have a lower density than the fluid (usually liquid), fluidization is achieved by the liquid moving downward to counter the net buoyancy force of the particles. Such a system is referred to the inverse fluidization (Fan et al., 1982). In the past decades, the advantages of the inverse fluidized bed (IFB) have been proven by many studies. Compared to the conventional upward fluidized bed, the inverse fluidization allows effective control of the process (Renganathan & Krishnaiah, 2004), high mass transfer rate (Nikolov & Karamanev, 1987), easy re-fluidization after sudden breakdown (Renganathan & Krishnaiah, 2003), etc. Especially, in the biological treatment of wastewater, the inverse fluidized bed is capable of controlling the biofilm thickness within a narrow range (Nikolov & Karamanev, 1987). As a result, the inverse fluidization is preferable in many biological processes such as the wastewater treatment, ferrous iron oxidation (Nikolov & Karamanev, 1987), and phenol biodegradation (Sabarunisha Begum & Radha, 2014).

In order to design, model and operate a pilot-scale fluidized bed, it is crucial to understand the hydrodynamic characteristics in the lab-scale reactor. In the past, many researchers have made efforts to study inverse fluidized beds. Fan et al. (1982) determined the flow patterns of the three-phase inverse fluidized bed and a modified model for predicting hydrodynamics. Later on, Karamanev and Nikolov investigated the bed porosity, minimum fluidization velocity, and correlations to predict bed expansion in an inverse fluidized bed (Karamanev & Nikolov, 1992). Ulaganathan and Krishnaiah proposed the three regimes of a liquid-solid inverse fluidized system, which are the packed bed, semi-fluidized bed, and fully-fluidized bed (Ulaganathan & Krishnaiah, 1996). Moreover, Femin Benedict et al. studied the effects of particle density and

Carboxymethyl cellulose (CMC) concentrations on the minimum fluidization velocity and bed expansion (Femin Bendict, Kumaresan, & Velan, 1998). In addition, Vijaya Lakshmi et al. discussed the relationship between the friction factor and solids loading and fluid viscosity (Vijaya Lakshmi et al., 2000).

Considering the merits of inverse fluidization, a new type of reactor has been developed in this study, named as the Gas-Driven Inverse Liquid-Solid Fluidized Bed (GDILSFB or GDFB for short). Unlike the commonly known liquid-solid fluidized beds, there is no continuous liquid flow in the GDFB (*Figure 2.1*). A baffle divides the column into two vertical sections, a riser and a downer. Gas is introduced into the riser and light particles are fluidized in the downer. Since the gas escapes to the atmosphere and does not enter the downer, the downer is believed to be a two-phase inverse fluidized bed. The goal of introducing this novel reactor is to achieve uniform fluidization with a relatively low energy consumption. To understand the GDFB and discover its potential applications, some basic hydrodynamics, including the fluidization regimes and bed expansion, are studied in this paper. Meanwhile, the effects of superficial gas velocity, solids loading, particle properties, and baffle opening on the hydrodynamics are discussed as well.

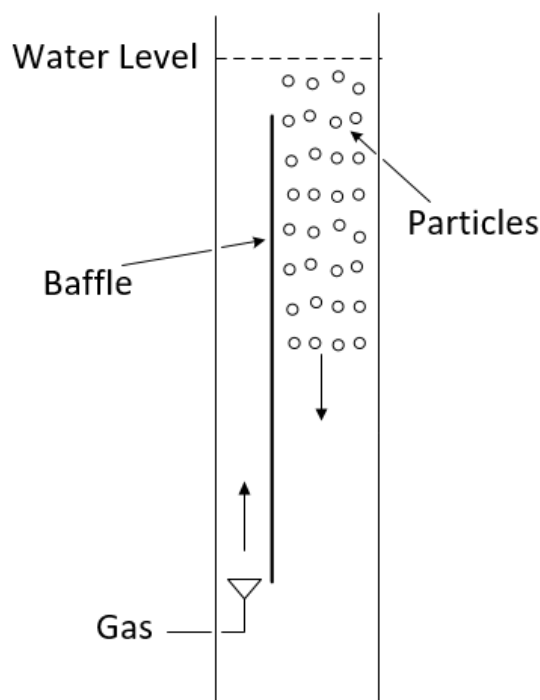


Figure 2.1 Simplified schematic diagram of the GDFB

2.2 Experimental Apparatus and Procedures

The schematic diagram of the GDFB and a cross-sectional view of the column is shown in *Figure 2.2*. The column has an inner diameter (ID) of 12.5 cm and its top is open to the atmosphere. A vertical baffle with a width of 10 cm and a length of 270 cm divides the column into two sections with unequal areas. The section with a smaller cross-sectional area is the riser and that with a larger area is defined as the downer. In the cross-sectional view of the column, point B represents the point at which the baffle crosses the ID perpendicularly, while point A and point C are end points of the ID. The ratio of line segments AB to BC is 1:4, which means that the baffle locates at the one-fifth point of the ID. Hence, the area of the downer is about six times the area of the riser. These two unequal areas are designed to lower the energy cost required for fluidization. Since the superficial gas velocity (U_G) is the quotient of gas flowrate divided by the area of the riser, for a certain gas flowrate, the smaller the area, the higher is the superficial gas velocity (U_G). Minimum gas amount is desired to drive more liquid to enter the downer. However, the area of riser should not be so small that the liquid is insufficient for entrainment by the wake of the bubbles. As a result, the above ratio of the riser and downer was chosen in this preliminary design of the GDFB. The area ratio of the riser to the downer can be varied depending on specific needs.

In this research, the gas and the liquid phases are air and tap water, respectively. At the bottom of the column, a liquid inlet valve allows water to be pumped from a tank into the column. Meanwhile, water can be discharged back to the tank through an outlet valve. A microporous gas distributor introduces air into the riser from the air supply and the flowrate is controlled by a calibrated rotameter. This gas distributor generates bubbles with a size of about 5 mm. When the air inlet valve is open, bubbles from the gas distributor rise upward in the riser, causing an upward liquid flow. Then, at the top of the riser, the gas escapes into the atmosphere, while the liquid form a downward flow in the downer due to the gravity. If the liquid velocity is sufficient, particles can be carried downward to achieve inverse fluidization. Several holes on the column wall at different altitudes allow the insertion of measuring devices such as optical fiber probe (OFP).

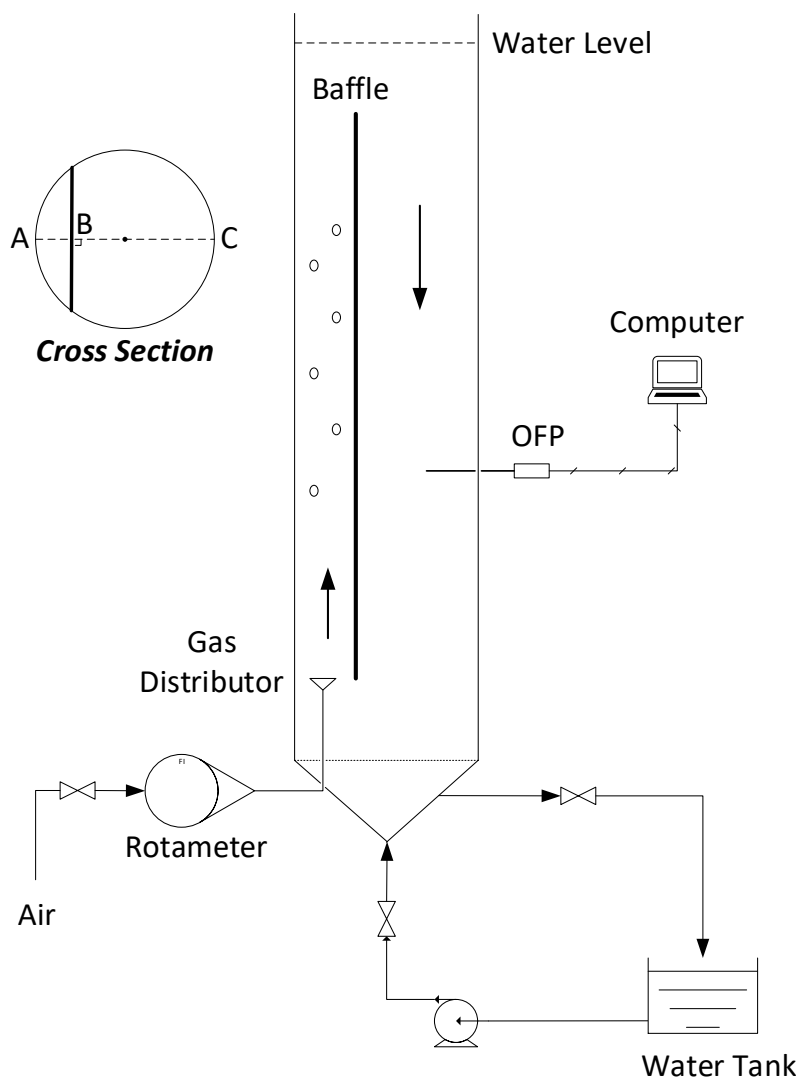


Figure 2.2 Schematic diagram of the GDFB and the cross-sectional view of column

The main variables of this study include particle properties (density, size, and shape), solids loading, and superficial gas velocity (U_G). Three types of light particles were used (Figure 2.3) and their properties are listed in Table 2.1. Particle size was measured by a vernier caliper and average equivalent diameter was taken for 50 particles. The terminal velocity of free rising particles is calculated from the equation:

$$U_t = \sqrt{\frac{4gd_p(\rho_L - \rho_P)}{3\rho_L C_D}} \quad (2.1)$$

$$C_D = \frac{432}{Ar} \left(1 + 0.0470Ar^{\frac{2}{3}} \right) + \frac{0.517}{1 + 154Ar^{-\frac{1}{3}}} \quad (2.2)$$

For light particles used in this research with $Ar > 1.18 \times 10^6 d_p^2$, $C_D = 0.95$ (Karamanev, 1996). Moreover, Solids loading is defined as the volumetric percentage that particles occupied in the total working volume, including the riser and downer. Hence, solids loading can represent the initial bed height before the onset of fluidization. The values of solids loading were chosen to be 5%, 10%, 15%, 20%, and 25%. The air rotameter controls the superficial gas velocity (U_G) and thus the bed expansion. Therefore, for each run, the superficial gas velocity (U_G) was adjusted and measurements were taken. Experiments were repeated at five solids loadings for each type of particles.

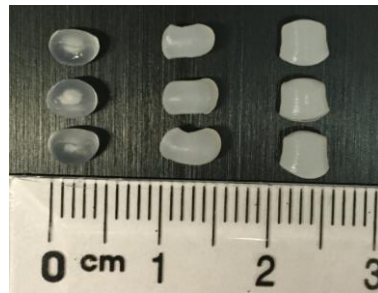


Figure 2.3 Photo of the particles used in the experiments

Table 2.1 List of particles and their properties

Material	Density ρ_p (kg/m ³)	Size d_p (mm)	Sphericity ϕ	Ar	Ut (cm/s)
Polypropylene (PP)	904	3.5	0.99	40522	6.81
Polyethylene (PE)	930	3.5	0.84	29496	5.81
Polypropylene (PP)	950	4.6	0.87	46900	5.61

Parameters to be determined are the initial fluidization velocity (U_{if}), uniform fluidization velocity (U_{uf}), bed expansion ratio (H/H_0), fluidization ratio (H_f/H_0), and fraction of packed bed (H_p/H). The initial fluidization velocity (U_{if}) and uniform fluidization velocity (U_{uf}) are determined by visual observation. The initial fluidization

velocity (U_{if}) is defined as the superficial gas velocity (U_G) at which particles in the lowest layer of the packed bed start to move downward, indicating the onset of fluidization. The uniform fluidization velocity (U_{uf}) is the superficial gas velocity (U_G) at which the packed bed no longer exists at the top of the downer.

Ambient temperature was applied for all the experiments. After water and particles were loaded into the column, the air inlet valve was opened and complete fluidization was maintained for about an hour to wet all the particles. Then, the gas was cut off and the upper level of the liquid-solid mixture (water level) was adjusted to 10 cm above the baffle. This action ensured that the working volume of each experiment was identical. At the beginning of each experiment, particles were completely fluidized and then the air flowrate was reduced gradually. The initial fluidization velocity (U_{if}) and uniform fluidization velocity (U_{uf}) could be obtained when the corresponding states were reached. Furthermore, by visual observation and a scale attached to the column, the initial bed height (H_0), total bed height (H), and packed bed height (H_p) were measured (*Figure 2.5*). Then, the bed expansion ratio (H/H_0), fluidization ratio (H_f/H_0), and fraction of packed bed (H_p/H) could be calculated from the recorded bed heights. For this newly invented GDFB, since the change of the total bed height has not been proven to demonstrate the same pattern as the fluidized bed height, both the bed expansion ratio (H/H_0) and fluidization ratio (H_f/H_0) would be studied.

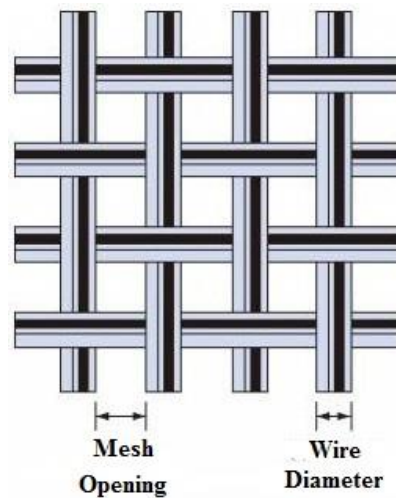


Figure 2.4 Enlarged mesh

In addition, to compare the impact of baffle structure on the hydrodynamics, another set of experiments was conducted in the GDFB using a baffle with mesh. The original system has a solid baffle with zero mesh opening, but a meshed baffle with 64% open area was installed in the alternative system. The opening of the meshed baffle was measured to be 0.4 mm and the wire diameter is 0.1 mm (*Figure 2.4*). In this case, only particles with a density of 930 kg/m^3 were studied and the solids loading ranged from 5% to 25%.

2.3 The Main System

2.3.1 The Inverse Fluidization Regimes

In the GDFB, four types of flow pattern can be observed as the increase of superficial gas velocity (U_G) (*Figure 2.5*). When the gas flowrate is low, particles suspend at the top of the downer without any movement since the density of particles is lower than that of water. This is called the packed bed. When the superficial gas velocity (U_G) reaches the initial fluidization velocity (U_{if}), particles in the lowest layer start to detach from the packed bed. As the gas velocity increases slightly, some particles remain in the packed bed while the other particles form a fluidized bed. This state refers to the semi-fluidized bed. By further increasing the gas velocity above the uniform fluidization velocity (U_{uf}), the packed bed disappears and the fully-fluidized bed is obtained. Furthermore, when the transition velocity (U_{tr}) is fulfilled, the fluidized bed will transform from the conventional regime to the circulating regime. In this case, particles occupy the entire downer and form a continuous flow around the baffle. This article focuses on the hydrodynamic behaviors of particles before entering the circulating regime.

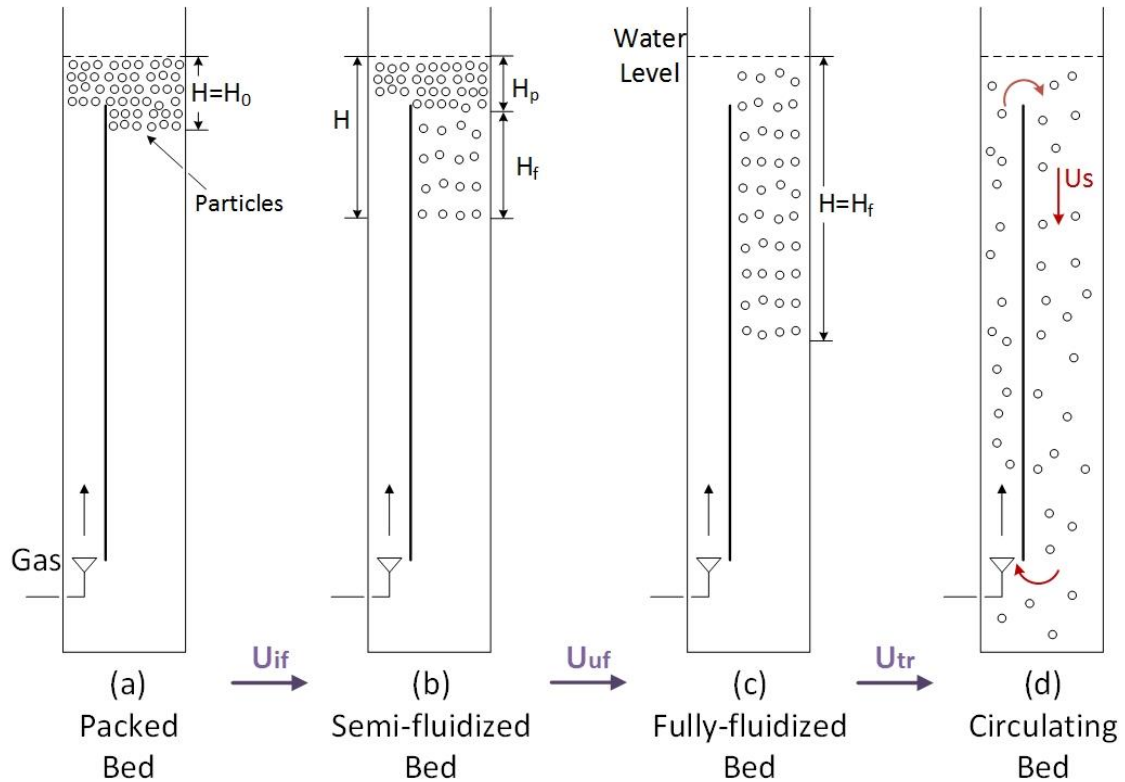


Figure 2.5 The inverse fluidization regimes in the main system

2.3.2 Initial and Uniform Fluidization Velocities

The initial fluidization velocity (U_{if}) indicates the onset of fluidization in the GDFB and is useful for finding the lowest gas flowrate to maintain the fluidization. The initial fluidization velocity (U_{if}) is plotted against the solids loading for the three types of particles (Figure 2.6). For all the particles, the initial fluidization velocity (U_{if}) increases with the increase of solids loading (initial bed height). Due to the structure of the GDFB, the driving force of fluidization is the downward flow of liquid from the riser. When particles are packed at the top of the downer, they hindered the liquid flow and the actual flowrate is reduced due to frictional loss. Thus, a higher solids loading results in a thicker fixed bed and more energy is lost when the liquid flow passes through the packed bed. Increasing the solids loading causes the increase of the superficial gas velocity (U_G) required for the onset of fluidization.

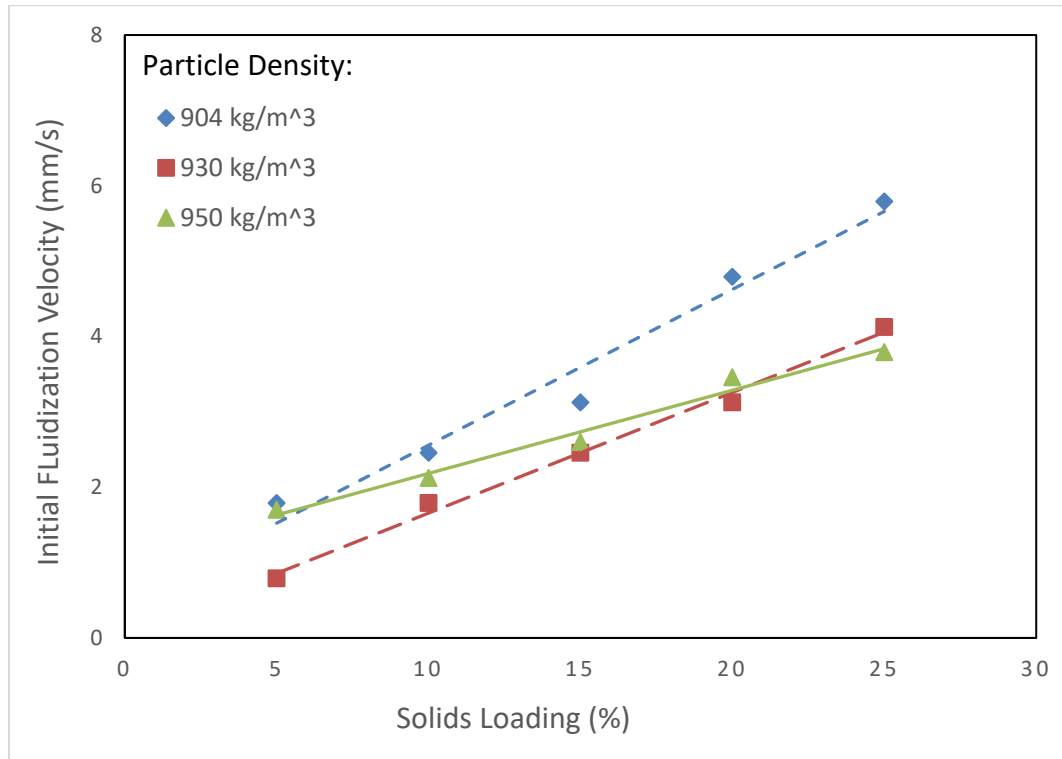


Figure 2.6 Initial fluidization velocity (U_{if}) versus solids loading for three types of particles in the main system.

Comparing the particles with a density of 904 kg/m^3 to particles with a density of 930 kg/m^3 , the higher the particle density, the higher is the initial fluidization velocity (U_{if}) as these two types of particles have the same size. This trend is similar to that in the upward fluidization and some former work done in the liquid-solid inverse fluidized bed (Femin Bendict et al., 1998; Vijaya Lakshmi et al., 2000). Since a lower particle density results in a larger buoyancy force, a larger downward force (liquid flow) is required to achieve the onset of fluidization (Femin Bendict et al., 1998). In addition, it is seen that particles with a density of 904 kg/m^3 and a diameter of 3.5 mm have a higher initial fluidization velocity (U_{if}) than particles with a density of 950 kg/m^3 and a diameter of 4 mm. Since a larger diameter results in a larger Archimedes number (Ar) and thus a larger buoyancy force (Vijaya Lakshmi et al., 2000), the initial fluidization velocity (U_{if}) should be proportional to the particle size. However, the initial fluidization velocity (U_{if}) is in

inverse proportion to the particle density as discussed above. Hence, only the effect of particle density on the hydrodynamics will be considered based on the comparison of particles with a density of 904 kg/m^3 and particles with 930 kg/m^3 . More experiments are needed to investigate the impacts of particle size and shape.

The uniform fluidization velocity (U_{uf}) refers to the state that all the particles are fluidized and the particle distribution in the bed is considered uniform. The plot of the uniform fluidization velocity (U_{uf}) versus the solids loading for three types of particles is shown in *Figure 2.7*. It is observed that the uniform fluidization velocity (U_{uf}) is proportional to the solids loading and inversely proportional to the particle density. Again, the particles with a density of 950 kg/m^3 should not be compared equally because its size is larger than the other two types. Since these trends of the uniform fluidization velocity (U_{uf}) are similar to that of the initial fluidization velocity (U_{if}), their causes can be explained with the same theories. Larger solids loading results in a higher uniform fluidization velocity (U_{uf}) because of the energy loss through the packed bed. On the other hand, particles with a higher density are subjected to a smaller buoyancy and thus requires a lower uniform fluidization velocity (U_{uf}) to realize fluidization. A similar result was reported by Ulaganathan and Krishnaiah that the minimum fluidization velocity (U_{mf}) increases with decreasing particle density (Ulaganathan & Krishnaiah, 1996). Since they defined the minimum fluidization velocity (U_{mf}) as the velocity required to achieve complete fluidization, the previous finding can be a verification of the current study.

The initial fluidization velocity (U_{if}) and the uniform fluidization velocity (U_{uf}) are two critical velocities during the developing progress of fluidization. According to the above discussion, achieving fluidization is easier for particles with a higher density and a smaller solids loading.

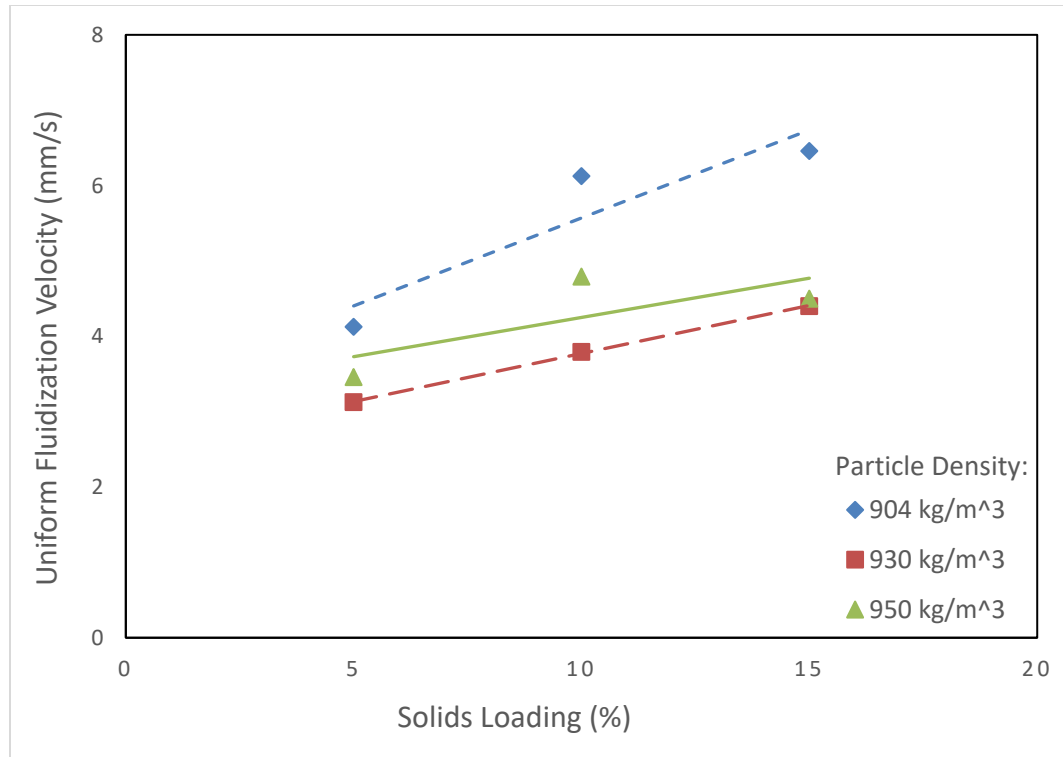


Figure 2.7 Uniform fluidization velocity (U_{uf}) versus solids loading for three types of particles in the main system.

2.3.3 Bed Expansion

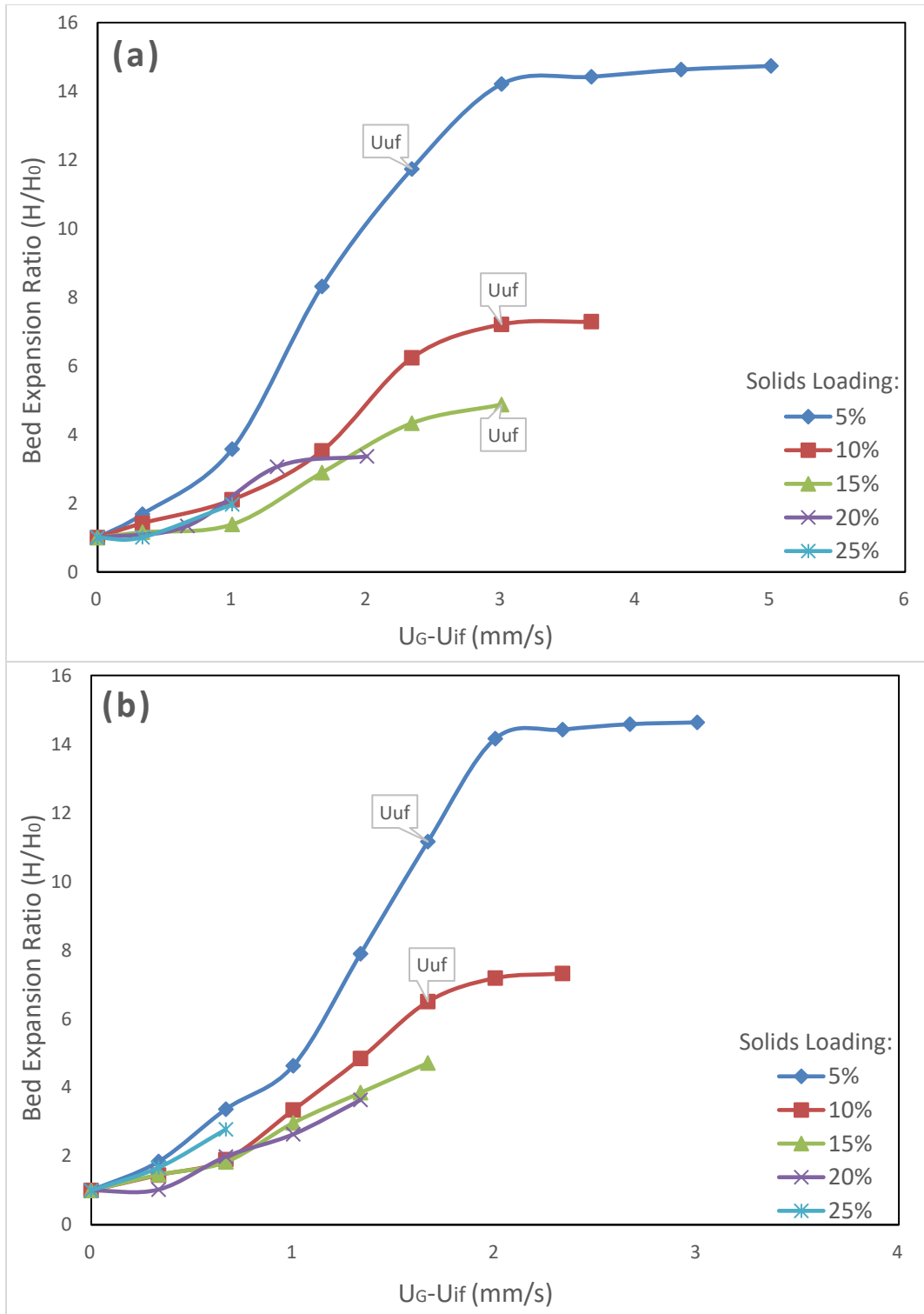
As the gas flowrate increases, the packed bed transforms to a semi-fluidized bed and finally develops the fully-fluidized bed. To incorporate the varying initial fluidization velocity (U_{if}), the excess superficial gas velocity ($U_G - U_{if}$) is introduced for the comparison of bed expansion. It is the difference between the superficial gas velocity (U_G) and the initial fluidization velocity (U_{if}). The bed expansion studies include the bed expansion ratio (H/H_0), fluidization ratio (H_f/H_0), and fraction of packed bed (H_p/H).

The bed expansion ratio (H/H_0) is obtained by dividing the total bed height (H) by the initial bed height (H_0). It is plotted against the excess superficial gas velocity ($U_G - U_{if}$) for three types of particles at different solids loadings (Figure 2.8). Since the initial fluidization velocity (U_{if}) is constant for a certain solids loading, the x-axis represents the change of the superficial gas velocity (U_G). Similarly, the fluidization ratio (H_f/H_0) is

plotted against the excess superficial gas velocity ($U_G - U_{if}$) in the *Figure 2.9*. For each type of particles at any solids loading, the bed expansion ratio (H/H_0) and the fluidization ratio (H_f/H_0) increase with the increase of the superficial gas velocity (U_G). The same trend of the bed expansion ratio (H/H_0) and the fluidization ratio (H_f/H_0) verified that the bed expansion was always positive. Therefore, the bed expansion ratio (H/H_0) is able to represent the fluidized bed height in the GDFB.

Furthermore, as the superficial gas velocity (U_G) increases, the rate of increase is slow at the beginning and after the uniform fluidization velocity (U_{uf}), while a relatively rapid increase is observed at the middle stage. However, this phenomenon is only obvious for solids loading less than 15%. Since the expanded bed height is limited by the total height of the column and a tiny increment of the gas velocity leads to a large increase of the bed height, the bed can only expand to a small ratio before particles start to circulate. Thus, the data points for higher solids loadings are not adequate to display the same pattern. At the beginning of the fluidization, the increment is slow because the driving force is reduced by friction between the liquid and the packed bed. As more particles are fluidized, the frictional loss is smaller and the actual flowrate is higher, which accelerates the bed expansion. The slow growth after reaching the uniform fluidization velocity (U_{uf}) may be explained by the limited height of the downer. Near the bottom of the downer, the liquid flow has to enter the riser and part of the downward driving force is lost again. Therefore, the expansion of the fluidized bed is constrained.

In addition, the increase of the bed expansion ratio (H/H_0) and fluidization ratio (H_f/H_0) at a lower solids loading is faster than that at a higher solids loading. Whereas, Ulaganathan and Krishnaiah reported that the dimensionless bed height (H/H_0) does not depend on the initial bed height in the two-phase inverse fluidized bed (Ulaganathan & Krishnaiah, 1996). As mentioned before, higher solids loading leads to a thicker packed bed and the actual liquid flowrate is lower. Therefore, the speed of the bed expansion would be faster in a system with a low solids loading.



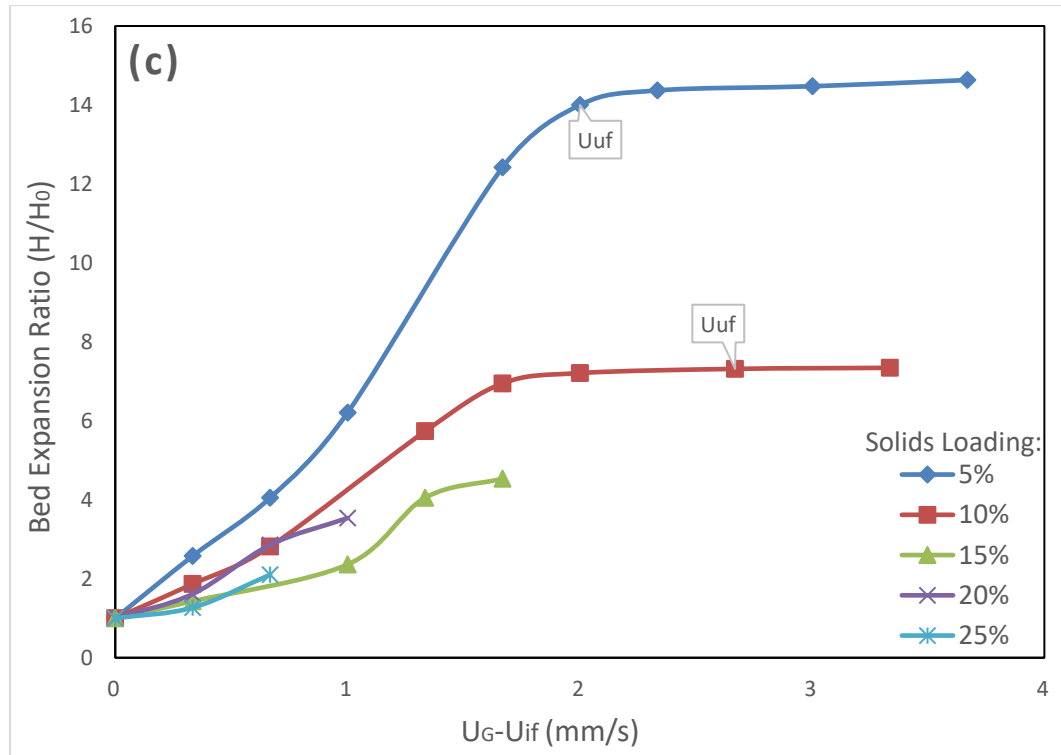
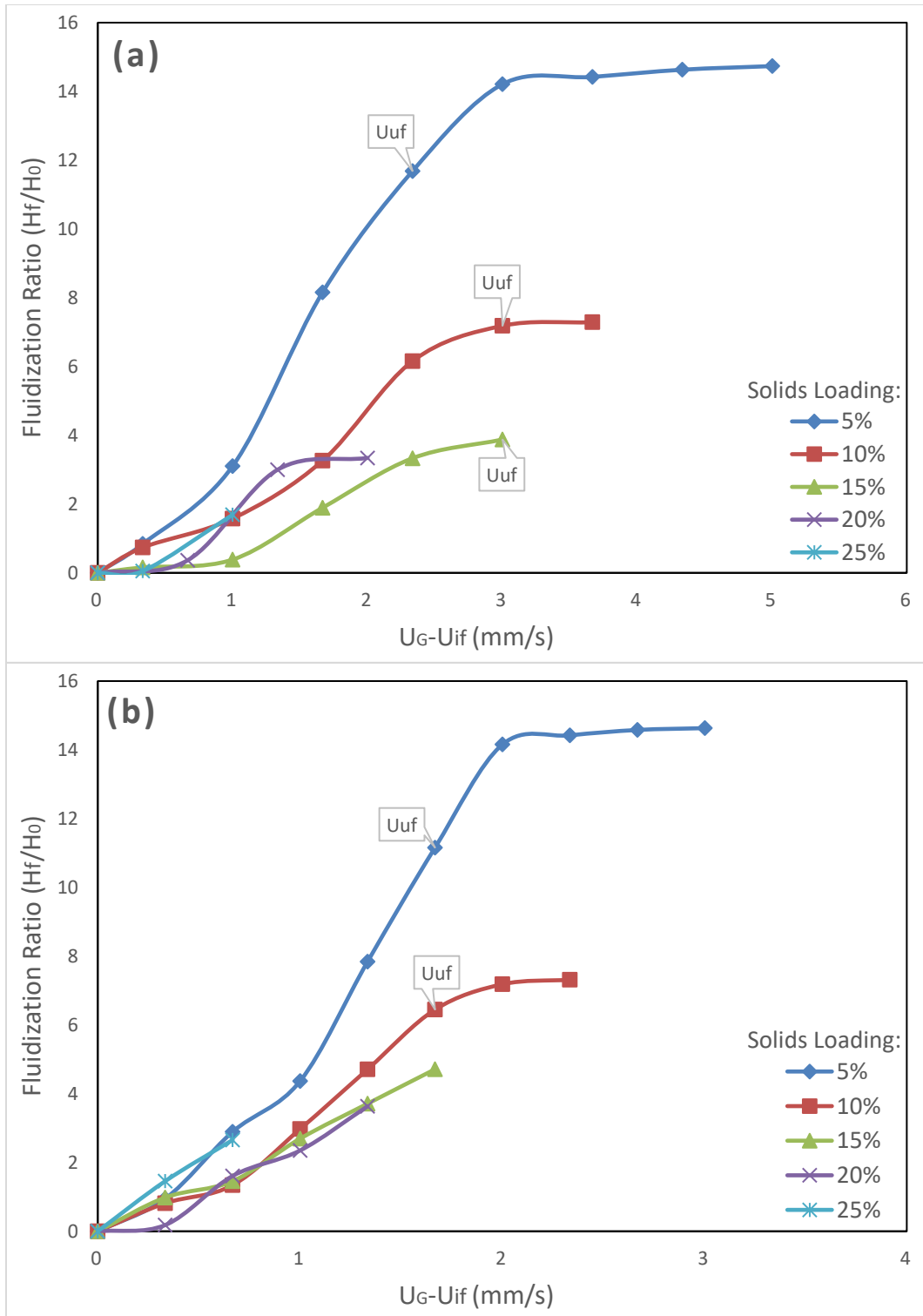


Figure 2.8 Bed expansion ratio (H/H_0) against the excess superficial gas velocity ($U_G - U_{if}$) at different solids loadings for particles with a density of (a) 904 kg/m^3 , (b) 930 kg/m^3 , and (c) 950 kg/m^3 in the main system.



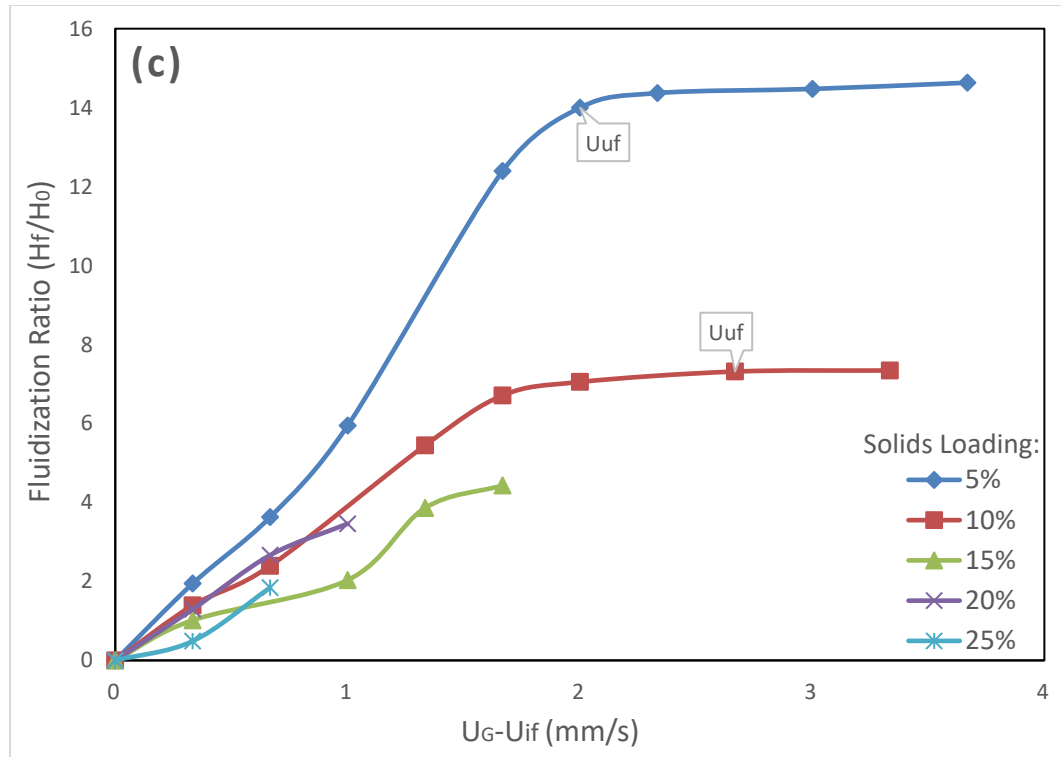
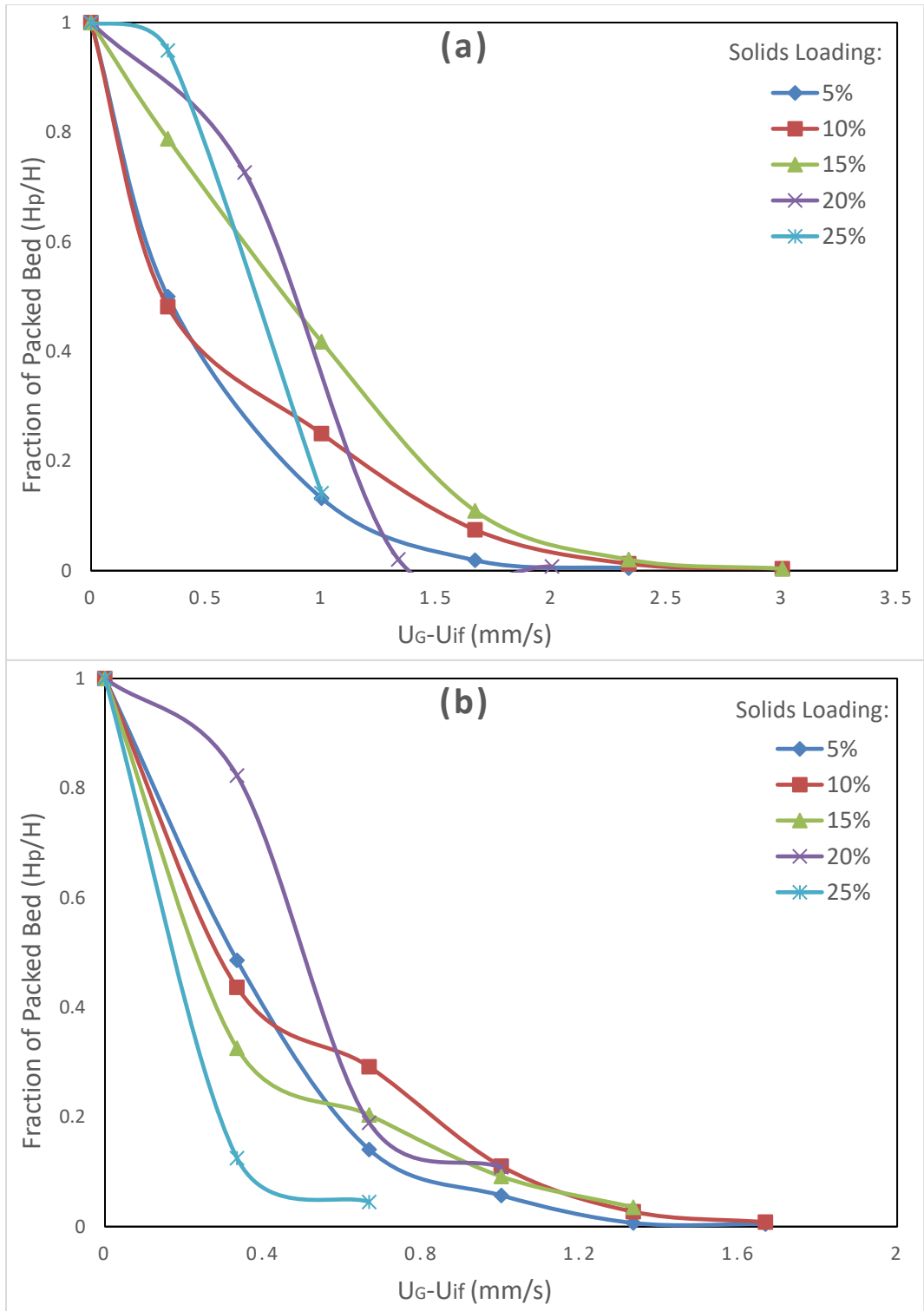


Figure 2.9 Fluidization ratio (H_f/H_0) against the excess superficial gas velocity ($U_G - U_{if}$) at different solids loadings for particles with a density of (a) 904 kg/m^3 , (b) 930 kg/m^3 , and (c) 950 kg/m^3 in the main system.

Moreover, since the bed expansion ratio (H/H_0) cannot demonstrate the variance of the packed bed, the fraction of packed bed (H_p/H) is discussed as well. The plots of the fraction of packed bed (H_p/H) versus the difference between the excess superficial gas velocity ($U_G - U_{if}$) for three types of particles at different solids loadings are shown in Figure 2.10. For each type of particles at the same solids loading, the fraction of packed bed (H_p/H) decreases with the increase of the superficial gas velocity (U_G). The superficial gas velocity (U_G) at which the fraction of packed bed (H_p/H) approaches zero is approximately the uniform fluidization velocity (U_{uf}). Nevertheless, a clear relationship between the fraction of packed bed (H_p/H) and the solids loading cannot be obtained from these plots. It is concluded that the packed bed height (H_p) decreases constantly as the superficial gas velocity (U_G) increases. More and more particles are gradually fluidized and suspended in the downer.



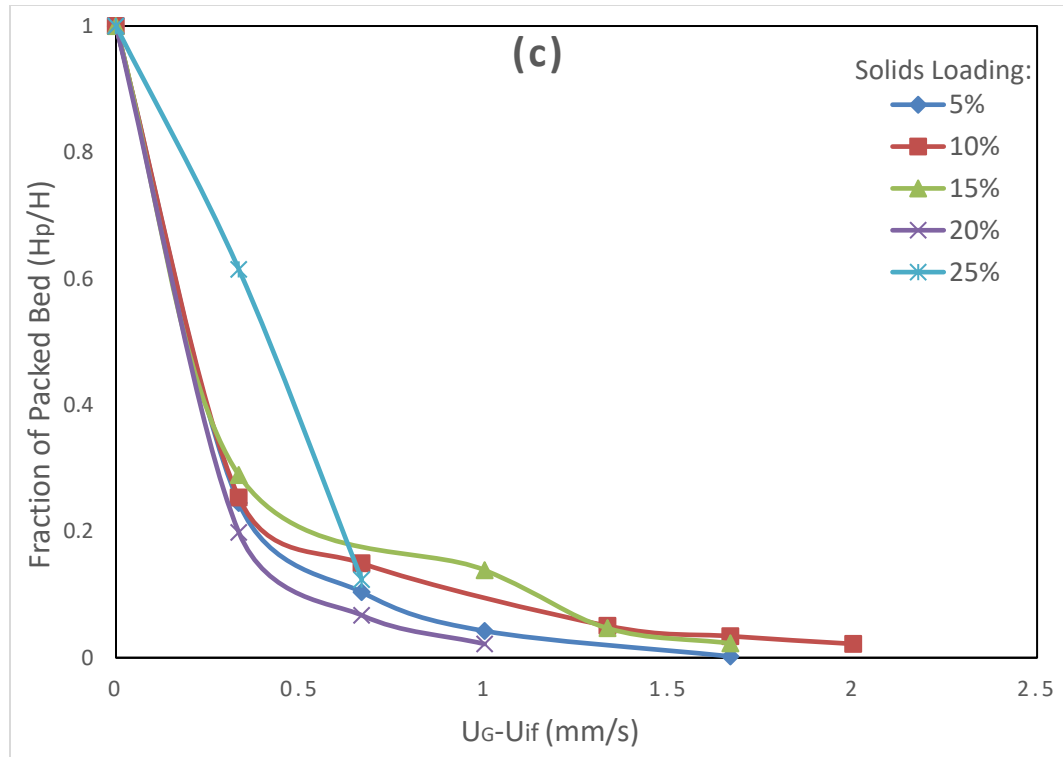


Figure 2.10 Fraction of packed bed (H_p/H) against the excess superficial gas velocity ($U_G - U_{if}$) at different solids loadings for particles with a density of (a) 904 kg/m^3 , (b) 930 kg/m^3 , and (c) 950 kg/m^3 in the main system.

In order to compare the effect of particle properties, the bed expansion ratio (H/H_0) versus the excess superficial gas velocity ($U_G - U_{if}$) is plotted on the same figure at 5%, 10%, and 15% solids loading (Figure 2.11). Considering the particles with the same diameter, the bed expansion ratio (H/H_0) of particles with a density of 930 kg/m^3 is larger than particles with a density of 904 kg/m^3 at the same solids loading. Hence, heavier particles would have larger bed expansion ratio (H/H_0). This result proves that particles with a higher density is easier to fluidize and more sensitive to changes in the superficial gas velocity (U_G).

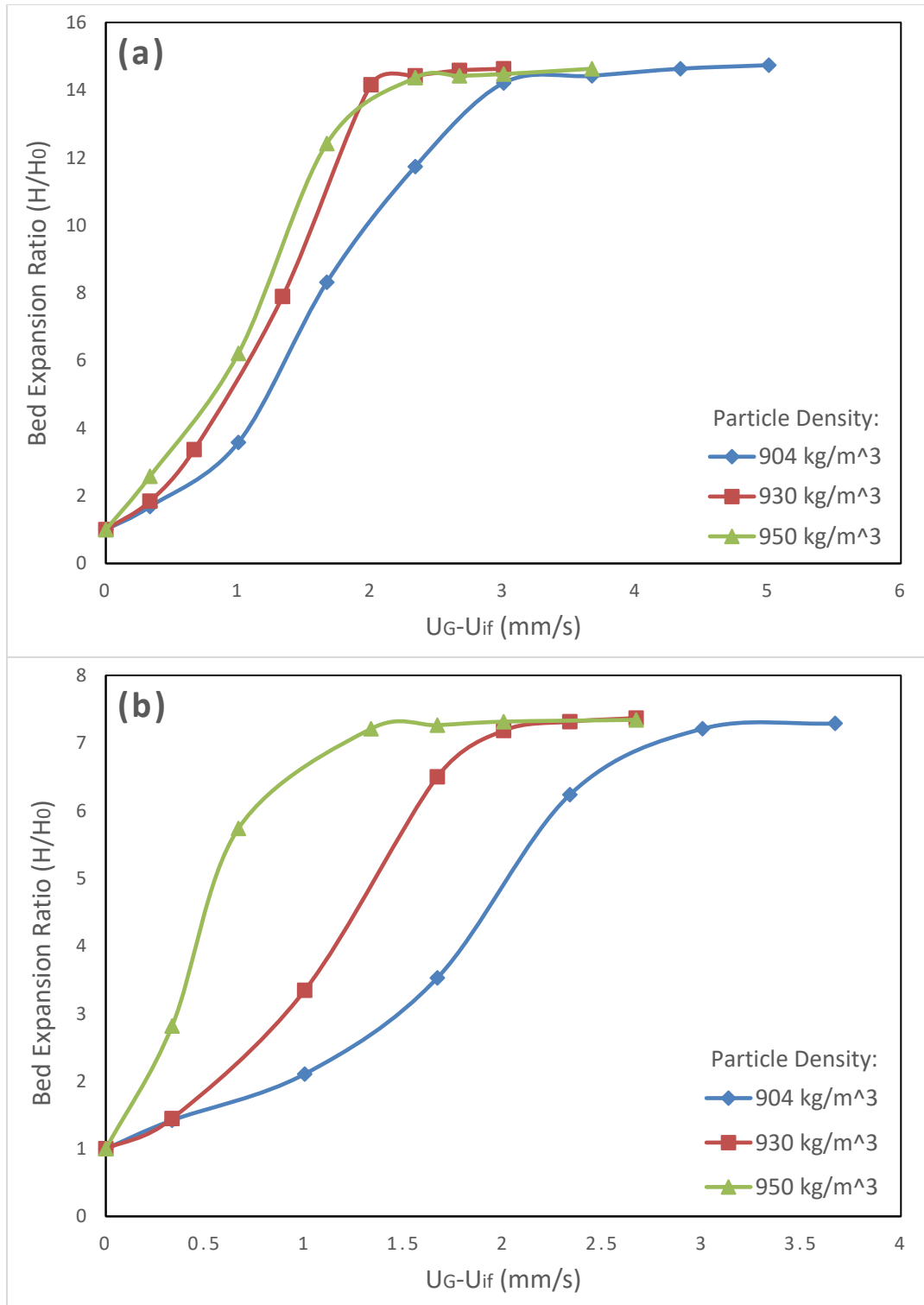


Figure 2.11 Bed expansion ratio (H/H_0) against the excess superficial gas velocity ($U_G - U_{if}$) for three types of particles at (a) 5% solids loading and (b) 10% solids loading in the main system.

The above findings on the bed expansion confirm the development of inverse fluidization regimes. At a low gas flowrate, the sum of the drag force and the gravitational force acting on the particles cannot exceed the net buoyancy force. Thus, the bed expansion ratio (H/H_0), the fluidization ratio (H_f/H_0), and the fraction of packed bed (H_p/H) remain unchanged. When the initial fluidization velocity (U_{if}) is reached, the fluidized bed height increases and the packed bed height decreases progressively until fluidization is achieved throughout the entire bed. In this case, the fluidized bed is considered uniform.

In addition, a linear relationship was found between the logarithms of the bed expansion ratio (H/H_0) and the excess superficial gas velocity ($U_G - U_{if}$) before the uniform fluidization. As shown in the *Figure 2.12*, the coefficient of determination (R^2) for each line is greater than 0.95, indicating that the trend lines fit the data series well. *Table 2.2* shows that the slope of the trend line decreases with increasing solids loading. However, since the bed expansion was influenced by particle properties and solids loading, it is difficult to find a single equation to express the linear relationship. Modelling would be necessary to acquire the exact expression, but the logarithms provide a useful hint for future work.

Table 2.2 Summary of linear relationship between the logarithms of bed expansion ratio ($\log_{10}(H/H_0)$) (y) and excess superficial gas velocity ($U_G - U_{if}$) (x)

Particle Density (kg/m^3)	Solids Loading	Linear Equation	R^2
904	5%	$y = 0.50x$	0.97
	10%	$y = 0.31x$	0.98
	15%	$y = 0.24x$	0.96
930	5%	$y = 0.66x$	0.98
	10%	$y = 0.50x$	0.99
	15%	$y = 0.43x$	0.99

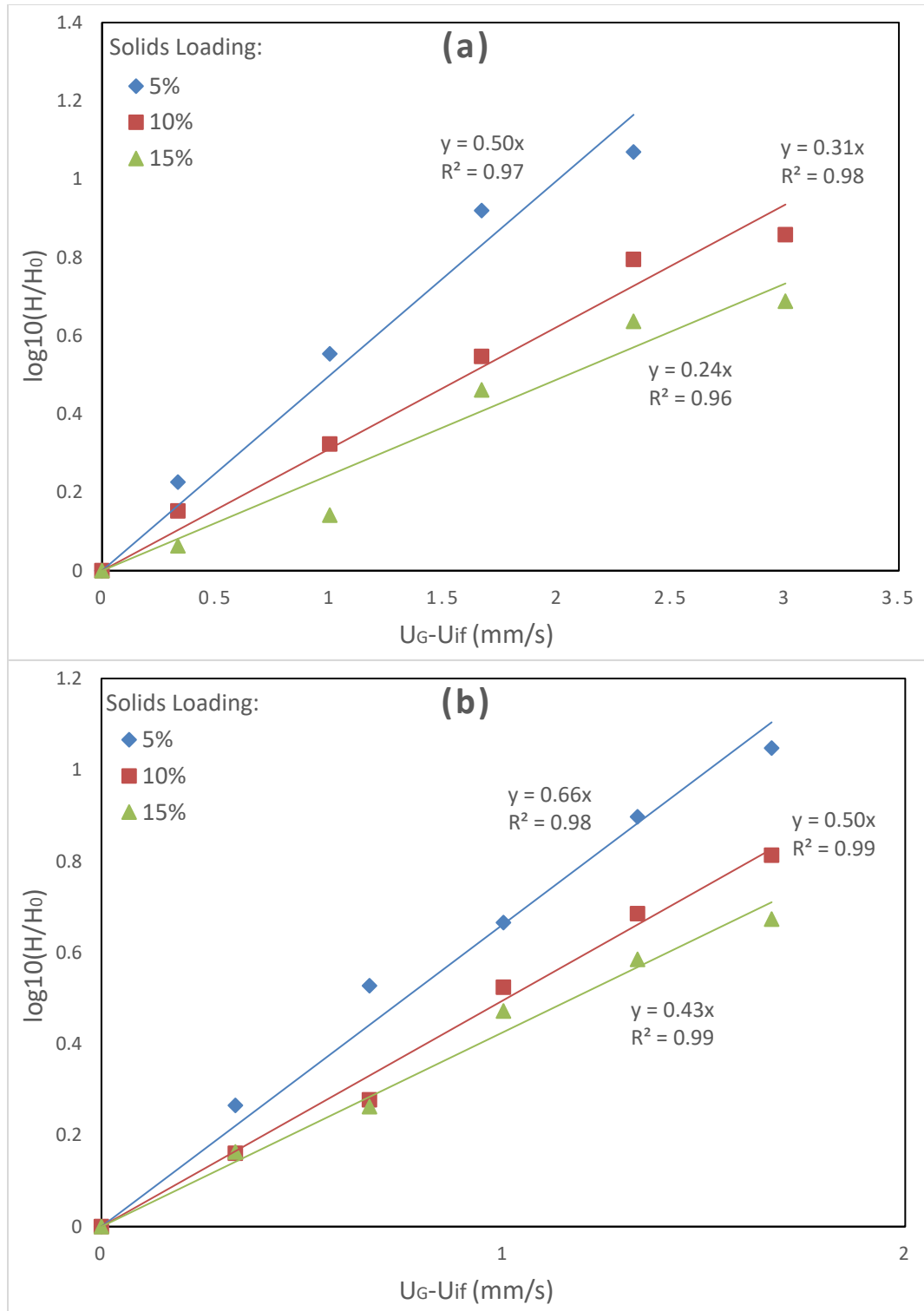


Figure 2.12 Logarithms of bed expansion ratio (H/H_0) against the excess superficial gas velocity ($U_G - U_{if}$) at 5%, 10%, and 15% solids loadings for particles with a density of (a) 904 kg/m^3 and (b) 930 kg/m^3 in the main system.

2.4 The Alternative System

2.4.1 The Inverse Fluidization Regimes

In the GDFB installed with a meshed-baffle, five types of flow pattern can be observed as the increase of superficial gas velocity (U_G) (*Figure 2.13*). When the gas flowrate is low, particles suspend at the top of the downer without any movement since the density of particles is lower than that of water. This is called the packed bed. When the superficial gas velocity (U_G) reaches the initial fluidization velocity (U_{if}), particles in the lowest layer start to detach from the packed bed. As the slight increase of gas velocity, some particles remain in the packed bed while the other particles form a fluidized bed. This state refers to the semi-fluidized bed. Then, the packed bed disappears and the fully-fluidized bed is obtained when the gas velocity is above the uniform fluidization velocity (U_{uf}). By further increasing the gas velocity, the fluidized bed moves downward as a whole and the upper boundary of the bed does not coincide with the water level. This pattern is named as the shifted bed, which is never observed in a solid-baffle system. Finally, when the transition velocity (U_{tr}) is fulfilled, the fluidized bed will transform from the conventional regime to the circulating regime. In this case, particles occupy the entire downer and form a continuous flow around the baffle. This paper focuses on the hydrodynamic behaviors of particles before entering the circulating regime.

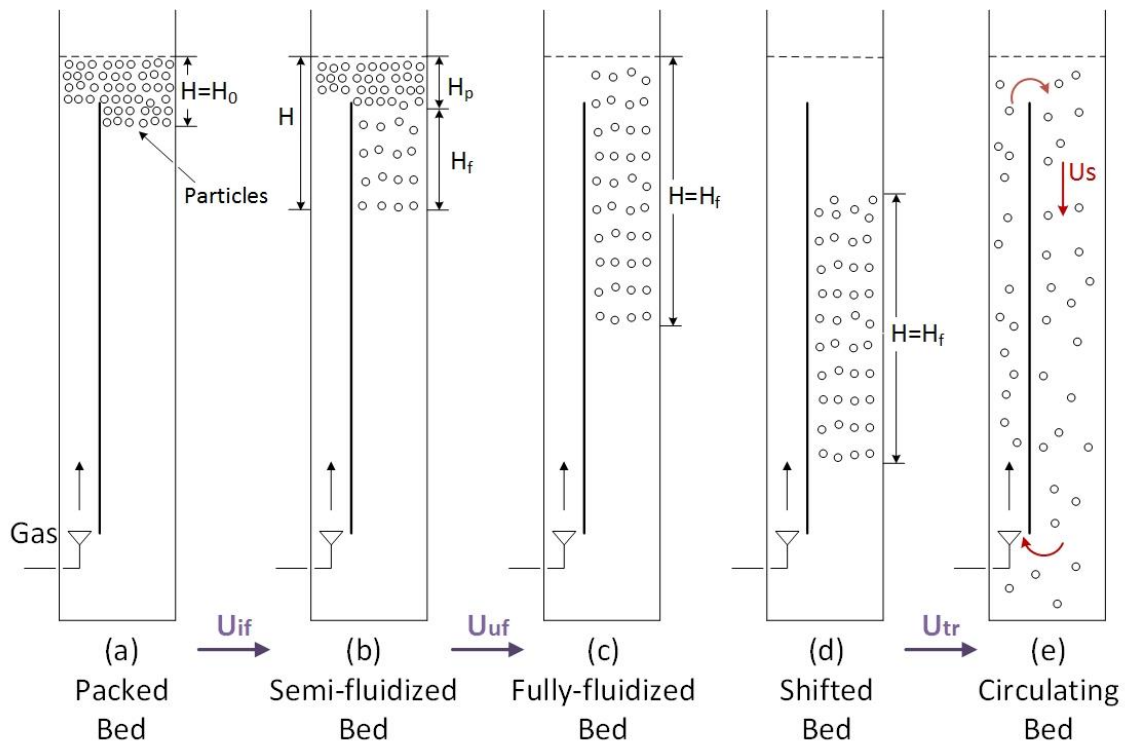


Figure 2.13 The inverse fluidization regimes in the alternative system

2.4.2 Initial and Uniform Fluidization Velocities

The initial fluidization velocity (U_{if}) is plotted against the solids loading for the systems with a solid baffle and a meshed baffle, respectively (Figure 2.14). Both sets of experiments used particles with a density of 930 kg/m^3 . When the baffle is with mesh, the solids loading has almost no effect on the initial fluidization velocity (U_{if}). In contrast, the initial fluidization velocity (U_{if}) is proportional to the solids loading for a solid-baffle system. As only the riser has bubbles rising upward, the pressure in the riser is lower than that in the downer. Due to this pressure gradient, some liquid passes through the mesh from the downer to the riser, creating a continuous liquid flow through the baffle. If a plenty of particles are packed at the top of the downer, this liquid flow can disturb the stationary state and help to fluidize the particles. Thus, the solids loading does not play an important role since the lower layers of the packed bed would be influenced by the liquid flow crossing the mesh.

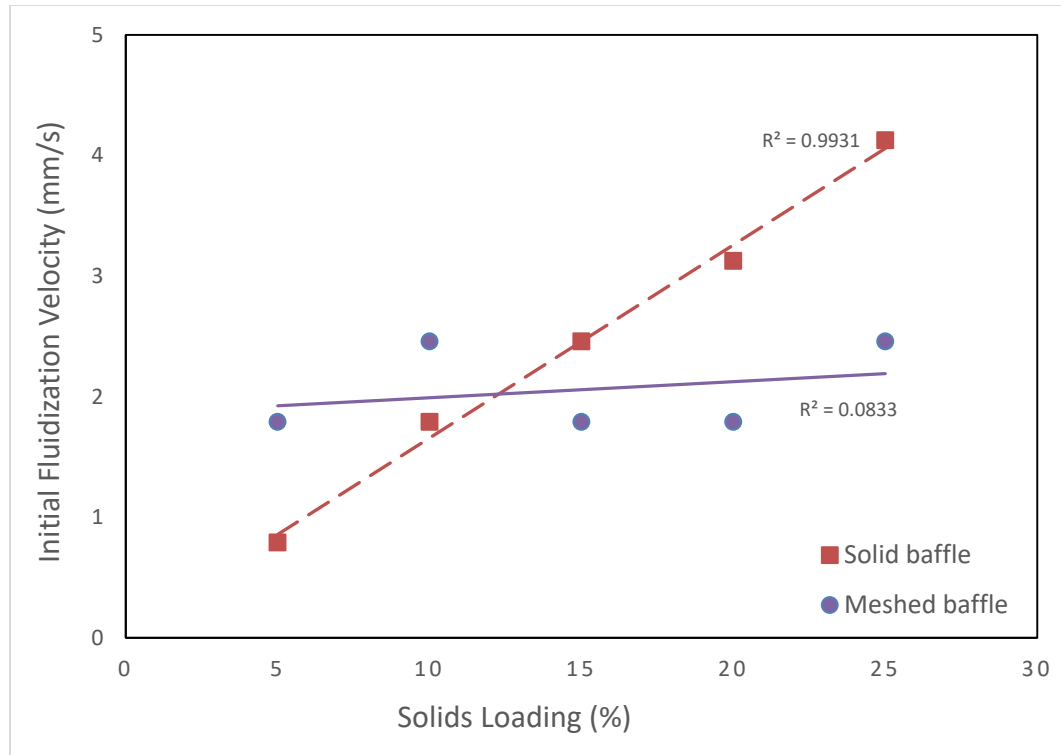


Figure 2.14 Initial fluidization velocity (U_{if}) versus solids loading for particles with a density of 930 kg/m^3 in the main system with solid baffle and in the alternative system with a meshed baffle.

The uniform fluidization velocity (U_{uf}) is plotted against the solids loading for the systems with a solid baffle and a meshed baffle, respectively (Figure 2.15). Unlike the initial fluidization velocity (U_{if}), the uniform fluidization velocity (U_{uf}) increases with the increase of solids loading for both the meshed-baffle system and the solid-baffle system. Since the initial fluidization velocity (U_{if}) refers to the state when the lowest layer of particles in the packed bed begin to move downward, the liquid flow crossing the mesh may help disturb the stationary state and obtain the onset of fluidization. In contrast, uniform fluidization is satisfied when particles at the top of the packed bed are fluidized, which is mainly driven by the liquid stream from the top of the riser. Thus, the uniform fluidization velocity (U_{uf}) in the meshed-baffle system demonstrates the same increasing trend as that in the solid-baffle system. The slight larger magnitude in the alternative system may be caused by the loss of some liquid flowrate through the mesh.

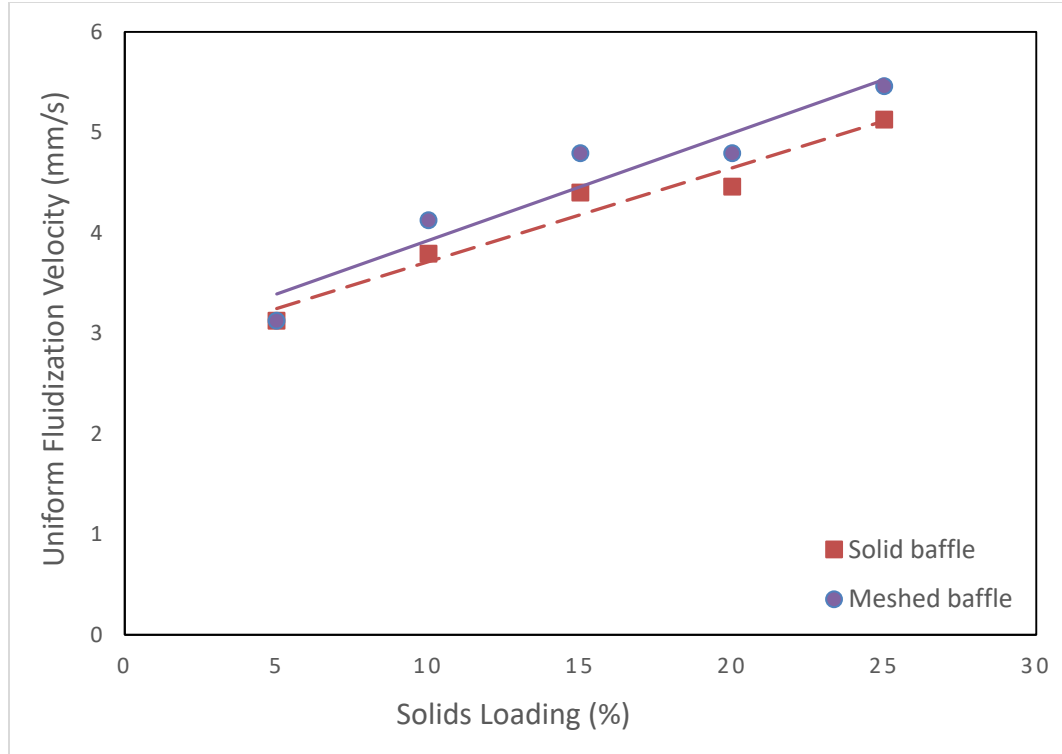


Figure 2.15 Uniform fluidization velocity (U_{uf}) versus solids loading for particles with a density of 930 kg/m^3 in the main system with solid baffle and in the alternative system with a meshed baffle.

2.4.3 Bed Expansion

In order to quantify the influences of mesh opening of the baffle, another set of experiments adopting a meshed baffle instead of a solid baffle was also conducted using the particles with a density of 930 kg/m^3 . The bed expansion ratio (H/H_0), fluidization ratio (H_f/H_0), and fraction of packed bed (H_p/H) are plotted against the excess superficial gas velocity ($U_G - U_{if}$) at five solids loadings (Figure 2.16, Figure 2.17, and Figure 2.18). It can be seen that the pattern of bed expansion with a meshed baffle is quite different from that with a solid baffle. The bed expansion ratio (H/H_0) and the fluidization ratio (H_f/H_0) do not follow a constant increase or decrease. As the superficial gas velocity (U_G) increases, the two ratios increase before reaching the uniform fluidization velocity (U_{uf}), but they decrease slightly after the uniform fluidization velocity (U_{uf}). Meanwhile, the fraction of packed bed (H_p/H) decreases with

increasing superficial gas velocity (U_G) until the packed bed no longer exists on the top of the downer.

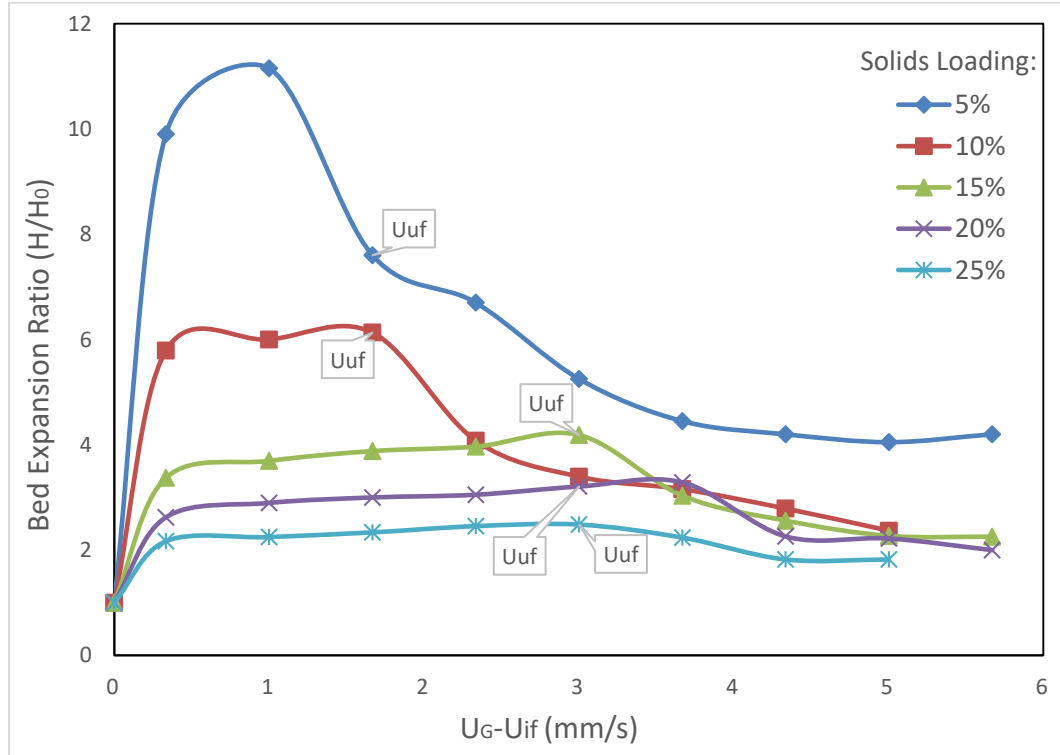


Figure 2.16 Bed expansion ratio (H/H_0) against the excess superficial gas velocity ($U_G - U_{if}$) at different solids loadings for particles with a density of 930 kg/m^3 in the alternative system.

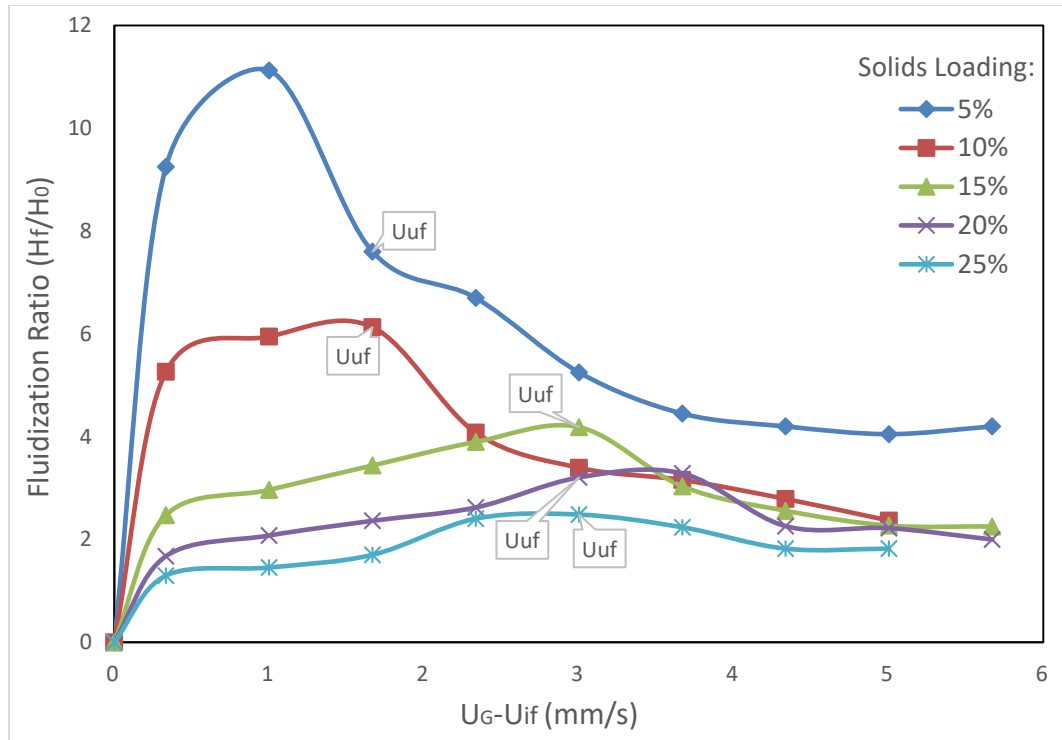


Figure 2.17 Fluidization ratio (H_f/H_0) against the excess superficial gas velocity ($U_G - U_{if}$) at different solids loadings for particles with 930 kg/m^3 in the alternative system.

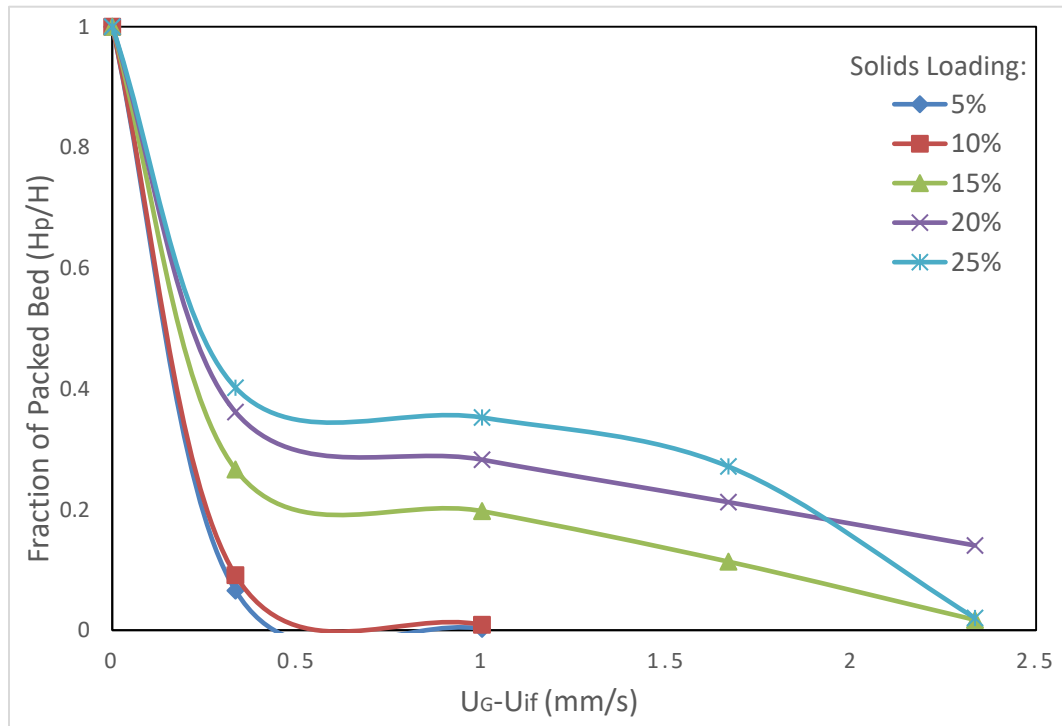


Figure 2.18 Fraction of packed bed (H_p/H) against excess superficial gas velocity ($U_G - U_{if}$) at different solids loadings for particles with 930 kg/m^3 in the alternative system.

The fluidization regimes can be applied to explain the above results. After the onset of fluidization is achieved, more and more particles are fluidized and the packed bed height decreases, which causes the increase of the total bed height. As the superficial gas velocity (U_G) further increases, particles are completely fluidized and then the entire bed would move downward. When the particles transform from the fully-fluidized bed to the shifted bed, the bed may be compressed, resulting in the decrease of the total bed height.

2.5 Conclusions

The fluidization regimes and bed expansion of the gas-driven inverse liquid-solid fluidized bed (GDFB) were studied experimentally in this article. To obtain the stable inverse fluidized bed in this reactor, a solid baffle is essential to control the orderly liquid flow. In such a system, as the gas flowrate increases, the four fluidization regimes include the packed bed, semi-fluidized bed, fully-fluidized bed, and circulating bed. The superficial gas velocities (U_G) required for the onset of fluidization and uniform fluidization are higher for larger solids loading and lower particle density. Moreover, the fluidized bed height and total bed height increase with the increasing gas flowrate, but the packed bed height decreases. The rate of bed expansion was found to be faster for heavier particles and for smaller solids loading, meaning that achieving fluidization is easier under these conditions. In brief, the bed expansion patterns have verified the observed fluidization regimes. This lab-scale GDFB requires low gas flowrates to operate, thus it is suitable for scale-up and applying to biochemical processes requiring low turbulence or low energy consumption.

Nomenclature

Ar	Archimedes number defined by $d_p^3 g(\rho_L - \rho_P)\rho_L/\mu_L^2$
C_D	Drag coefficient
d_p	Particle diameter (mm)
g	Gravitational acceleration on earth (m/s^2)
H_0	Initial bed height (cm)
H	Total bed height (cm)
H_p	Packed bed height (cm)
H/H_0	Bed expansion ratio
H_f/H_0	Fluidization ratio
H_p/H	Fraction of packed bed
ID	Inner diameter of the column (cm)
U_G	Superficial gas velocity (cm/s)
U_{if}	Initial fluidization velocity (cm/s)
U_t	Terminal velocity of particles (cm/s)
U_{tr}	Transition velocity (cm/s)
U_{uf}	Uniform fluidization velocity (cm/s)

Abbreviations

GDFB	Gas-driven inverse liquid-solid fluidized bed
IFB	Inverse fluidized bed

OFP Optical fiber probe

PE Polyethylene

PP Polypropylene

Greek letters

μ_L Liquid viscosity being 1.002×10^{-3} Pa.s at 20°C (Pa.s)

ρ_L Liquid density (kg/m³)

ρ_P Particle density (kg/m³)

ϕ Particle sphericity

Subscripts

0 Initial packed bed

f Fluidized bed

G Gas

if Initial fluidization

L Liquid

P Particle

tr Transition

uf Uniform fluidization

References

- Fan, L., Muroyama, K., & Chern, S.-H. (1982). Hydrodynamic Characteristics of Inverse Fluidization in Liquid-Solid and Gas-Liquid-Solid Systems. *The Chemical Engineering Journal*, 24, 143–150.
- Femin Bendict, R. J., Kumaresan, G., & Velan, M. (1998). Bed expansion and pressure drop studies in a liquid-solid inverse fluidised bed reactor. *Bioprocess Engineering*, 19, 137–142.
- Karamanev, D. G. (1996). Equations for calculation of the terminal velocity and drag coefficient of solids spheres and gas bubbles. *Chemical Engineering Communications*, 147, 75–84.
- Karamanev, D. G., & Nikolov, L. N. (1992). Bed Expansion of Liquid-Solid Inverse Fluidization. *AIChE Journal*, 38(12), 1916–1922.
- Nikolov, L., & Karamanev, D. (1987). Experimental Study of the Inverse Fluidized Bed Biofilm Reactor. *The Canadian Journal of Chemical Engineering*, 65(April 1987), 214–217.
- Renganathan, T., & Krishnaiah, K. (2003). Prediction of Minimum Fluidization Velocity in Two and Three Phase Inverse Fluidized Beds. *The Canadian Journal of Chemical Engineering*, 81(August), 853–860.
- Renganathan, T., & Krishnaiah, K. (2004). Liquid phase mixing in 2-phase liquid-solid inverse fluidized bed. *Chemical Engineering Journal*, 98(August 2003), 213–218. <http://doi.org/10.1016/j.cej.2003.08.001>
- Sabarunisha Begum, S., & Radha, K. V. (2014). Hydrodynamic behavior of inverse fluidized bed biofilm reactor for phenol biodegradation using *Pseudomonas fluorescens*. *Korean Journal of Chemical Engineering*, 31(3), 436–445. <http://doi.org/10.1007/s11814-013-0260-z>
- Sang, L. (2013). *Particle Fluidization in Upward and Inverse Liquid-Solid Circulating*

Fluidized Bed.

Ulaganathan, N., & Krishnaiah, K. (1996). Hydrodynamic characteristics of two-phase inverse fluidized bed. *Bioprocess Engineering*, 15, 159–164.

Vijaya Lakshmi, A. C., Balamurugan, M., Sivakumar, M., Newton Samuel, T., & Velan, M. (2000). Minimum fluidization velocity and friction factor in a liquid-solid inverse fluidized bed reactor. *Bioprocess Engineering*, 22, 461–466.

Chapter 3

3 Gas-Driven Inverse Liquid-Solid Fluidized Bed with Circulation

3.1 Introduction

Traditionally, when the density of solid particles is higher than that of the fluid, fluidization is realized by a gas or liquid flowing opposite to the direction of gravity. In contrast, particles with a lower density than the fluid (usually liquid) are fluidized by the downward liquid stream countering the net buoyancy force of the particles. This kind of system is named as the inverse fluidization (Fan et al., 1982). It has been proved that inverse fluidized beds have many advantages over the upward fluidized beds. For instance, inverse fluidization provides high mass transfer rate (Nikolov & Karamanev, 1987), easy re-fluidization after breakdown (Renganathan & Krishnaiah, 2003), and efficient control of the process (Renganathan & Krishnaiah, 2004). Thus, it has been applied to various biological processes, including phenol biodegradation (Sabarunisha Begum & Radha, 2014) and ferrous iron oxidation (Nikolov & Karamanev, 1987). Particularly, inverse fluidization allows the control of biofilm thickness within a narrow range in biological wastewater treatment (Nikolov & Karamanev, 1987).

On the other hand, circulating fluidized beds have several advantages, comparing to conventional fluidized beds. For example, back-mixing of phases is significantly reduced and the interfacial contact efficiency is increased (Zhu et al., 2000). As a result, upward liquid-solid circulating fluidized beds (LSCFB) have been applied to some industrial fields. For instance, a pilot-scale LSCFB was applied to remove biological nutrient from municipal wastewater (Chowdhury et al., 2009). The continuous recovery of proteins from cheese whey was achieved by adopting the LSCFB in the ion exchange system (Lan et al., 2000). Moreover, the LSCFB was introduced to realize the enzymatic polymerization of phenol (Trivedi et al., 2006) and to produce lactic acid by extractive fermentation (Patel et al., 2008). In terms of hydrodynamic behaviors in the LSCFB, the radial distributions of solids holdup and liquid velocity were found to be non-uniform (Liang et al., 1996) and the comprehensive fluidization regimes were proposed (Liang et

al., 1997). Then, Zheng et al. studied the uniformity of axial particle distribution, critical transition velocity, and conditions for stable operation (Zheng et al., 1999). Zheng and Zhu also defined the onset velocity for the circulating fluidization regime, which depends on particles properties instead of operating conditions (Zheng & Zhu, 2001).

Recently, Huang and Zhu developed the Gas-Driven Inverse Liquid-Solid Fluidized Bed (GDILSFB or GDFB) (Huang & Zhu, 2017). The column is composed of a downer and a riser, vertically separated by a baffle (*Figure 3.1*). Inverse fluidization is driven by a gas stream from the bottom of the riser instead of a continuous liquid flow. When the gas flowrate is adequate, light particles are fluidized in the downer. By further increasing the gas flowrate, particles can cross the bottom of the baffle and enter the riser. If particles are able to maintain a continuous flow between the riser and the downer, the conventional regime is considered to be transformed to the circulating regime. To benefit the future applications of this reactor, some hydrodynamic behaviors of particles circulating in the GDFB have been investigated. Specifically, this study focuses on the transition velocity and average particle velocity and their relationship with the superficial gas velocity, solids loading, particle properties, and baffle structure. The aim is to discover the optimum operating conditions of this reactor with low energy costs.

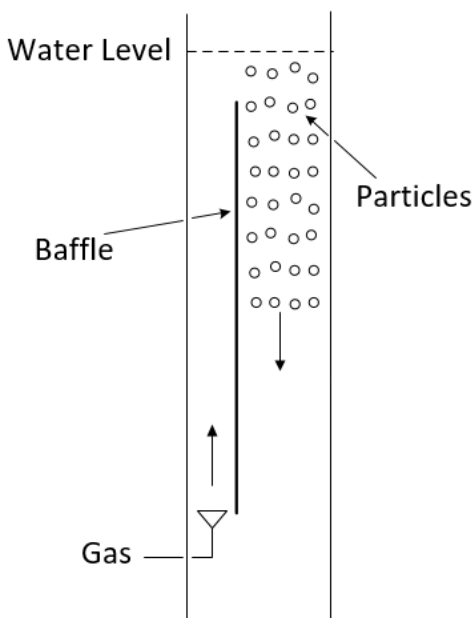


Figure 3.1 Sketch of the GDFB

3.2 Materials and Methods

3.2.1 Experimental Apparatus and Procedures

Figure 3.2 shows a sketch of the gas-driven inverse liquid-solid fluidized bed (GDFB) and its cross-sectional view. The top of the column is open to the air and the inner diameter (ID) of the column is 12.5 cm. The column is divided into a riser and a downer by a baffle with a length of 270 cm and a width of 10 cm. The riser refers to the vertical section having a smaller cross-sectional area and the downer is the one with a larger area. As shown in the cross section of the column, end points of the ID are point A and point C, while the baffle crosses the ID perpendicularly at point B. The length of line segment BC is 4 times that of line segment AB. Thus, the area of the downer is about one-sixth of the area of the riser. The purpose of designing these two different areas is to achieve fluidization with a relatively low energy cost. For a given gas flowrate, a smaller area of the riser results in a higher superficial gas velocity (U_G) and more liquid can be entrained by a smaller gas amount. Nevertheless, the riser cannot be too small that the total liquid amount constraint the liquid flow entering the downer. Therefore, in this preliminary design, the areas of the downer and riser were selected to have a six times difference.

The liquid and gas in this research are tap water and air, respectively. Water is pumped into the column from a tank through a liquid inlet valve at the bottom of the GDFB. Meanwhile, an outlet valve allows water to be discharged back to the tank. Air is introduced into the riser from air supply via the gas distributor and a calibrated rotameter controls the flowrate. Bubbles coming out of the gas distributor move upward in the riser, which results in a liquid stream flowing upward. The gas reaching the top of the riser is released into the atmosphere, but the liquid flows downward in the downer because of the gravity. Particles would be carried downward when the liquid flowrate satisfies the condition for the onset of fluidization. Additionally, measuring devices, such as the optical fiber probe, can be inserted into the column through a few holes on the wall at various altitudes.

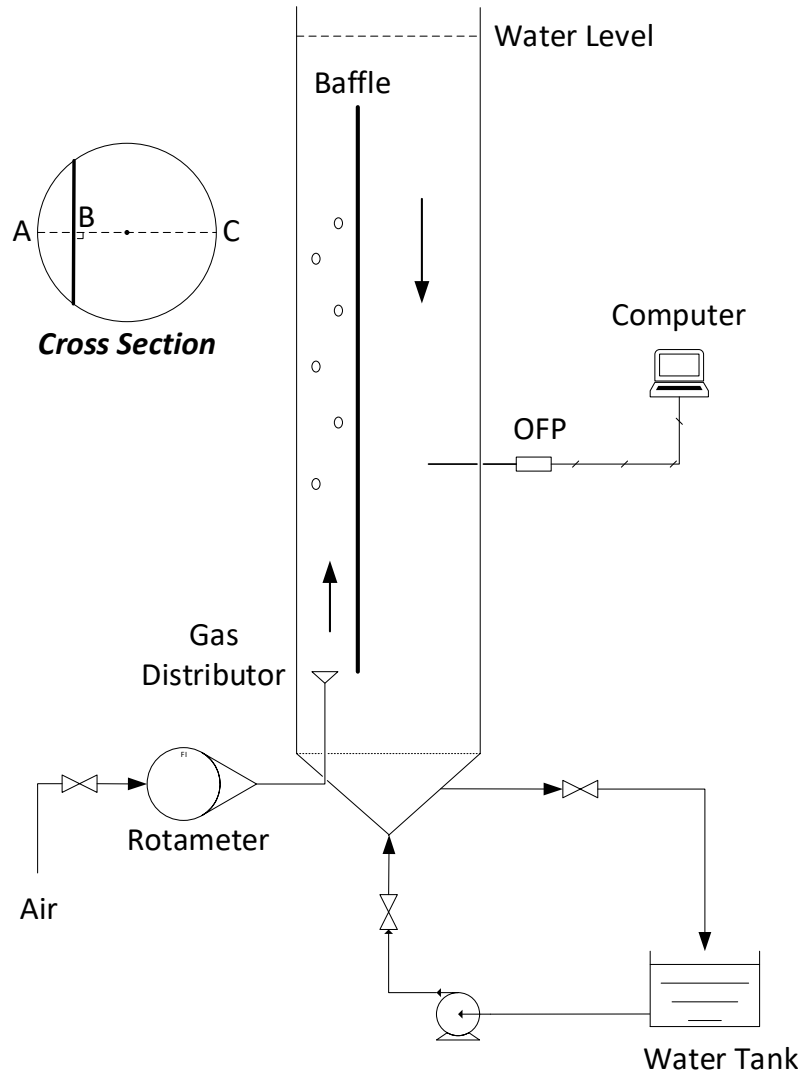


Figure 3.2 Schematic drawing of the GDFB and the cross section of column

Three variables in this research are particle properties (size, shape, and density), solids loading, and superficial gas velocity (U_G). Figure 3.3 is a photo of light particles used in the experiments and their properties are shown in the Table 3.1. Vernier caliper was used to measure the particle size and average equivalent diameter of 50 particles was adopted. For free rising particles, the terminal velocity is obtained using the following equations:

$$U_t = \sqrt{\frac{4gd_p(\rho_L - \rho_P)}{3\rho_L C_D}} \quad (3.1)$$

$$C_D = \frac{432}{Ar} \left(1 + 0.0470Ar^{\frac{2}{3}} \right) + \frac{0.517}{1 + 154Ar^{-\frac{1}{3}}} \quad (3.2)$$

Since the above particles have $Ar > 1.18 \times 10^6 d_p^2$, $C_D = 0.95$ should be applied (Karamanev, 1996). Furthermore, solids loading is the percentage that the volume of particles occupied in the entire working volume (both the riser and downer). Before the onset of fluidization, solids loading reflects the initial bed height. The solids loadings were selected to be 5%, 10%, 15%, 20%, and 25%. The superficial gas velocity (U_G) was controlled by the air rotameter, which indirectly controls the bed expansion. Hence, the superficial gas velocity (U_G) was adjusted and measurements were taken for each run. The experiments were repeated for three types of particles at five solids loadings.

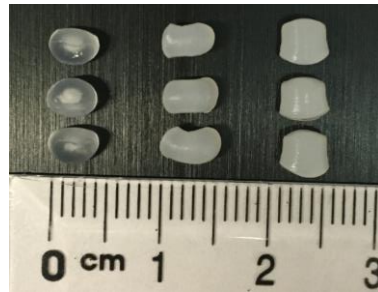


Figure 3.3 Photo of particles used in this study

Table 3.1 List of particles and their properties

Particle Type	Material	Density ρ_p (kg/m ³)	Size d_p (mm)	Sphericity ϕ	Ar	Ut (cm/s)
A	Polypropylene (PP)	904	3.5	0.99	40522	6.81
B	Polyethylene (PE)	930	3.5	0.84	29496	5.81
C	Polypropylene (PP)	950	4.6	0.87	46900	5.61

The transition velocity (U_{tr}) and average particle velocity (U_p) were determined when particles form the circulating bed in the GDFB. The transition velocity (U_{tr}) is defined as the minimum superficial gas velocity (U_G) required for the transformation from the

conventional fluidized regime to the circulating regime. It is observed visually and recorded when the corresponding state is reached. The average particle velocity (U_p) is simply the average velocity of particles circulating in the downer of the GDFB, measured by an optical fiber probe (OFP) and the details will be explained in the following.

All the experiments were conducted under the ambient temperature. The OFP was inserted into the downer and its data collecting program was started. After feeding particles and water into the reactor, particles were kept circulating for around one hour, which helps to wet the particles. To ensure the same working volume for each experiment, the water level (the upper boundary of the liquid-solid mixture) was set to 10 cm above the baffle. Particles were fully fluidized at the beginning of each experiment and then the gas flowrate was gradually increased. The transition velocity (U_{tr}) was obtained at the onset of circulation and average particle velocity (U_p) was determined by the OFP after the circulating regime was reached. Measurement by the OFP was taken at seven selected superficial gas velocities (U_G).

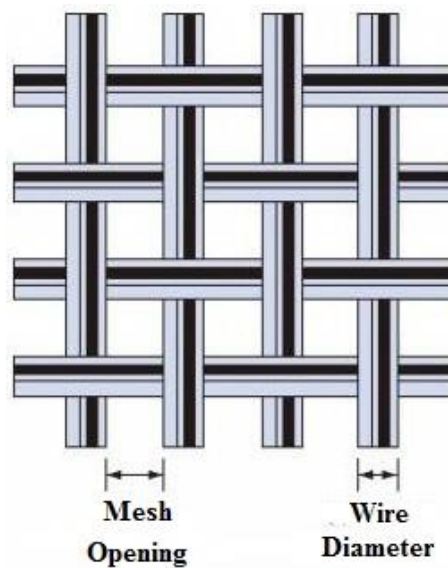


Figure 3.4 Enlarged mesh

Moreover, another set of experiments was performed installing a baffle with mesh in the GDFB to compare the effect of baffle structure on the hydrodynamic behaviors. The open area percentage of this meshed baffle is 64% while the main system originally has a solid baffle with no opening. The measured mesh opening is 0.4 mm and the diameter of the

wire is 0.1 mm (*Figure 3.4*). In this situation, the five solids loadings from 5% to 25% were studied, but the only selected type of particles was the one with a density of 930 kg/m³.

3.2.2 Optical Fiber Probe (OFP)

The optical fiber probe (OFP) with light-transmitting fibers is model PV-6, manufactured by the Institute of Process Engineering, Chinese Academy of Sciences. Its circular tip has a diameter of 3.8 mm and the spacing between two light receiving channels is 1.4 mm. As illustrated in *Figure 3.5*, light is emitted from the light source to particles in the downer and reflected back to the receiving fibers. Then, the photomultiplier and Analog/Digital converter transform the light into electrical impulses and output the signal as voltage ranging from 0 to 5 V to a computer. As a result, the output voltage, or the intensity of reflected light, is proportional to the volumetric concentration of particles (Sang, 2013).

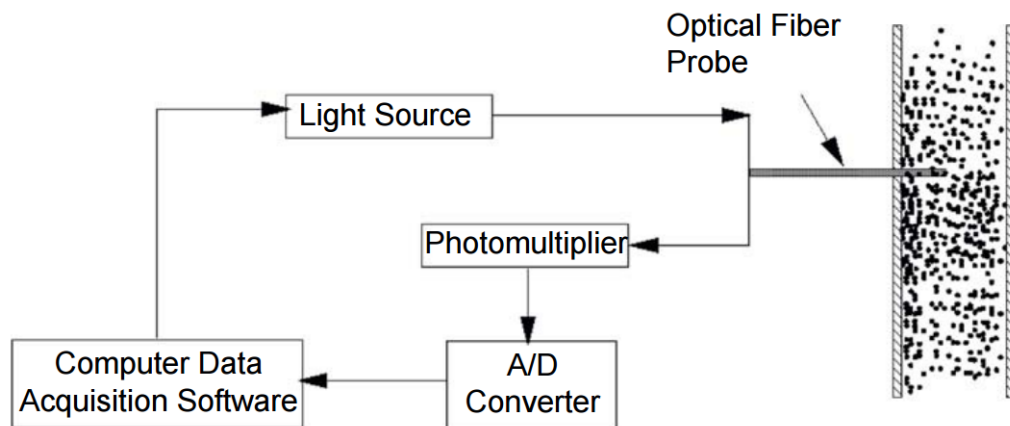


Figure 3.5 OFP diagram for particle velocity measurement (Sang, 2013)

When a particle passes the two channels, a signal peak is generated in each channel. Since the one channel was held at a higher vertical position than the other during the experiments, a time lag exists between the corresponding peaks of the two channels. The particle velocity (U_p) can be calculated by the following equation:

$$U_p = \frac{L_e}{T_{AB}} \quad (3.3)$$

L_e is the effective distance between the two channels, which is 1.4 mm for PV-6 model, and T_{AB} represents the time lag between signals received by the two channels. Since the signal peaks are very similar, it is necessary to apply the cross correlation theory to identify the corresponding pairs and obtain the proper time interval (T_{AB}). The cross correlation (ϕ_{AB}) is described in the following equation:

$$\phi_{AB} = \lim_{T \rightarrow \infty} \frac{1}{T} \int_0^T A(t)B(t + \tau)dt \quad (3.4)$$

In the above equation, when signals from the two channels are matched to yield the maximum cross correlation (ϕ_{AB}), the time lag (T_{AB}) is obtained (Sang, 2013). In this study, the axial position of the OFP was at 150 cm above the bottom of the baffle. The tip of the probe inserted into the downer was 5 cm from both the wall of the column and the baffle perpendicularly (*Figure 3.6*). Therefore, the probe can be considered at the center of the downer to avoid the impact of the column wall on the particle behaviors.

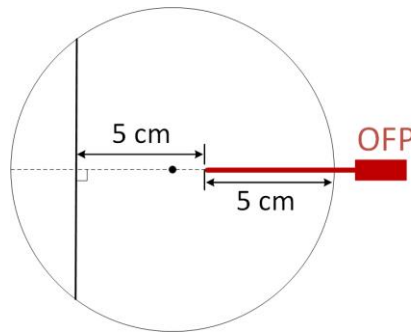


Figure 3.6 Cross-sectional view of the column with the radial position of the OFP

3.3 The Main System

3.3.1 The Fluidization Regimes

In the gas-driven inverse liquid-solid fluidized bed (GDFB), four fluidization regimes can be distinguished as the superficial gas velocity (U_G) increases (*Figure 3.7*). Since

particles has a lower density than water, particles suspend statically at the top of the downer when the gas velocity is low. This pattern refers to the packed bed. When the initial fluidization velocity (U_{if}) is reached, particles in the lowest layer of the packed bed begin to detach and move downward. The state that some particles forming the packed bed while the others are fluidized is called the semi-fluidized bed. As the gas velocity increases above the uniform fluidization velocity (U_{uf}), the packed bed no longer exists and particles form the fully-fluidized bed. As the gas velocity reaches the transition velocity (U_{tr}), particles enter the riser from the bottom of the downer and return to the downer passing over the top of the baffle. The circulating bed is obtained if the continuous flow of particles can be maintained. The current study emphasizes on the transition velocity (U_{tr}) and average particle velocity (U_p) under the circulating regime.

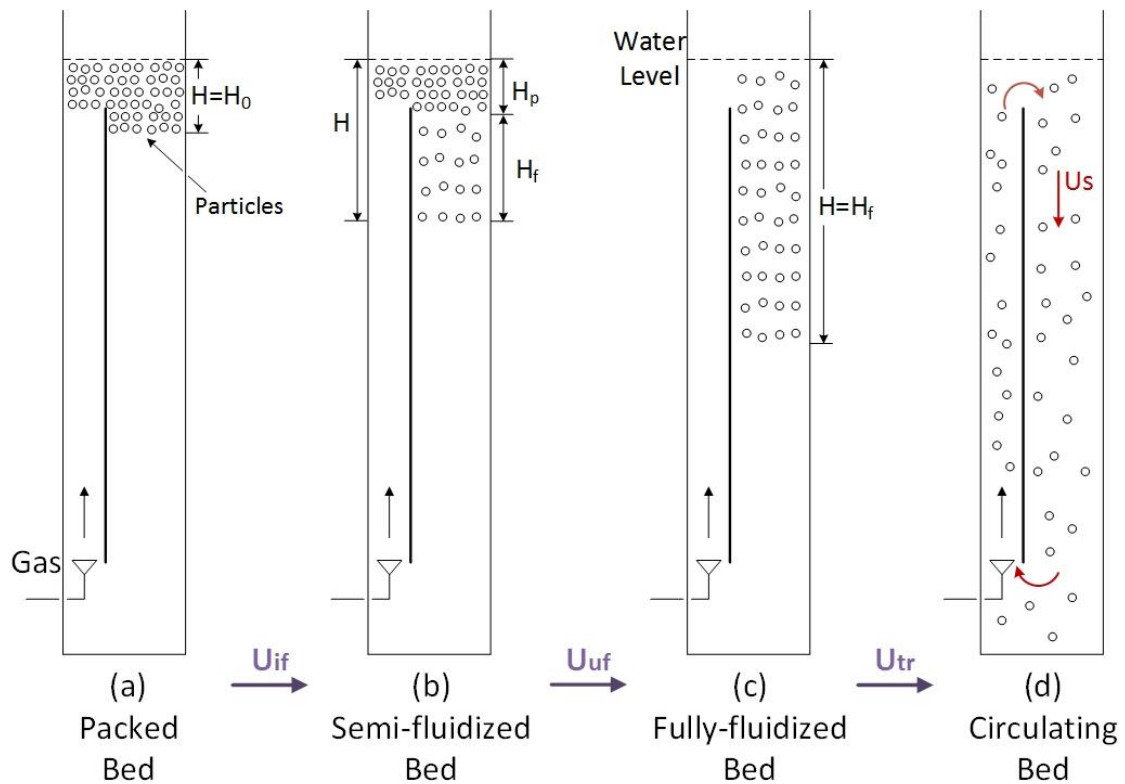


Figure 3.7 The fluidization regimes of the GDFB in the main system

3.3.2 Transition Velocity

The transition velocity (U_{tr}) indicates the transformation from the conventional regime to the circulating regime. With a superficial gas velocity (U_G) higher than the transition velocity, particles will circulate around the baffle continuously. The transition velocity (U_{tr}) is plotted against solids loading for three types of particles in *Figure 3.8*. For the particles with a density of 904 kg/m^3 and 930 kg/m^3 , the transition velocity (U_{tr}) does not have a close relationship with the solids loading. For particles with a density of 950 kg/m^3 , a slight decrease is observed as the solids loading increases. Since the density of this type of particles is very close to the density of water and the column height is not infinite, a small increase of the gas flowrate can lead to particles entering the riser for a large amount of particles. Overall, it can be concluded that solids loading has almost no impact on the transition velocity (U_{tr}). When all the particles are fluidized, the forces acting on each particle can be considered the same throughout the bed. Thus, each particle requires the same drag force to be carried downward and the solids loading does not affect the transition velocity (U_{tr}).

On the other hand, the transition velocity (U_{tr}) of particles with a density of 904 kg/m^3 is larger than that of 930 kg/m^3 . Since these two types of particles have the same size, the transition velocity (U_{tr}) is higher for particles with a higher density. Since a lower particle density results in a larger buoyancy force, a larger downward force (liquid flowrate) is required to achieve the circulating regime. In addition, it is seen that particles with a density of 904 kg/m^3 and a diameter of 3.5 mm have a larger initial fluidization velocity (U_{if}) than particles with a density of 950 kg/m^3 and a diameter of 4.6 mm. Since a larger diameter results in a larger Archimedes number (Ar) and thus a larger buoyancy force (Vijaya Lakshmi et al., 2000), the transition velocity (U_{tr}) should be proportional to particle size. However, the transition velocity (U_{tr}) is in inverse proportion to the particle density as discussed above. Hence, more experiments are needed to verify the effect of particle size. In this study, particles with a density of 950 kg/m^3 are not compared equally to particles with a density of 904 kg/m^3 and 930 kg/m^3 .

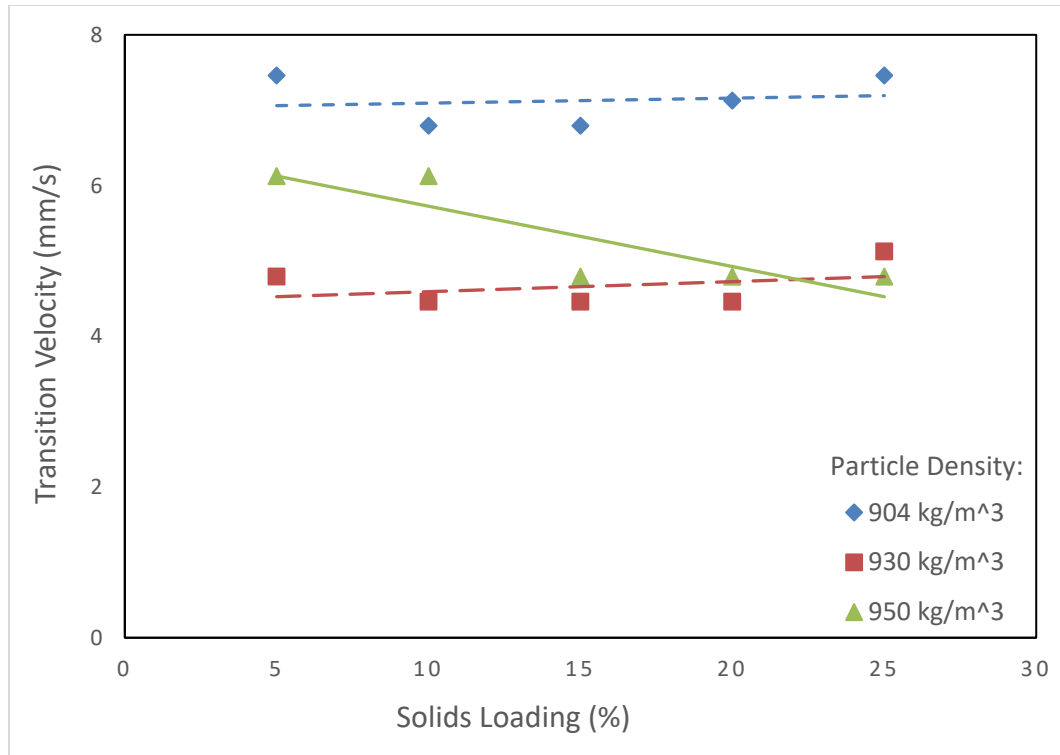


Figure 3.8 Transition velocity (U_{tr}) against solids loading for three types of particles in the main system.

3.3.3 Average Particle Velocity

The plots of the average particle velocity (U_p) versus the superficial gas velocity (U_G) for three types of particles at different solids loadings are shown in *Figure 3.9*. For any type of particles at a certain solids loading, the average particle velocity (U_p) is proportional to the superficial gas velocity (U_G). Increasing the gas flowrate causes the increase of liquid flowrate in the downer and the drag force acting on the particles. The average velocity of particles circulating in the reactor would be accelerated by increasing the net force.

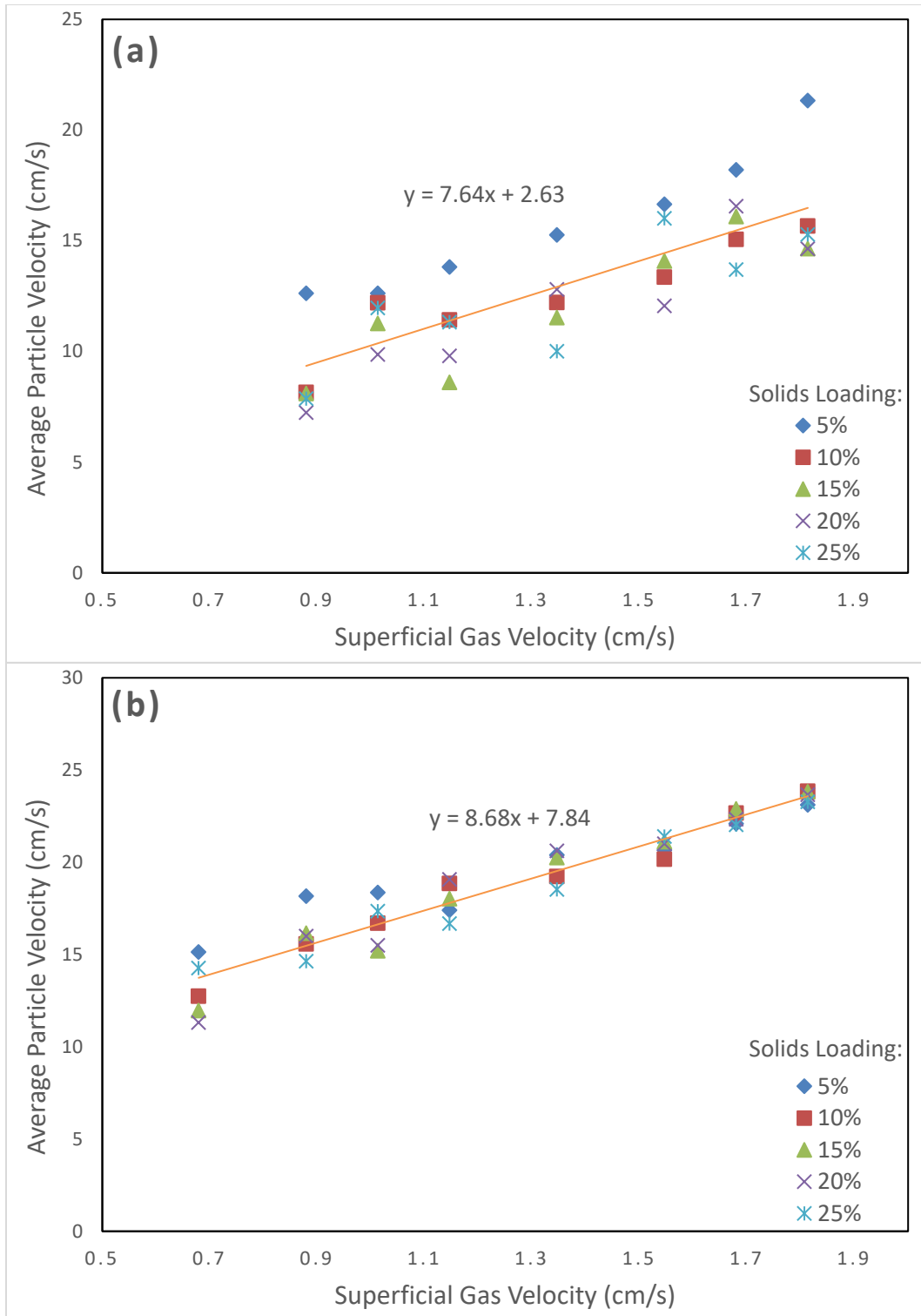
Moreover, based on the overlap of the data points, solids loading does not have a noticeable effect on the average particle velocity (U_p). The straight trend line in each plot represents the average velocity of all five solids loadings. The maximum deviation of data points from the average line for particles with a density of 904 kg/m³, 930 kg/m³, and 950 kg/m³ is 35%, 18%, and 28%, respectively. The relatively high deviation for

particles with a density of 904 kg/m^3 is mainly caused by the high average particle velocity (U_P) at 5% solids loading. This result may be caused by the fluctuation of pressure in the air supply. According to the ideal gas law ($PV = nRT$), the decrease of pressure leads to the increase of volumetric gas flowrate and thus the increase of drag force on the particles. Theoretically, solids loading should not influence the average particle velocity (U_P) because particles fluidized in the downer experience the same net drag force.

A linear equation can be obtained for each type of particles to predict the average particle velocity (U_P) based on the superficial gas velocity (U_G). Combining these equations and the dimensions of this lab-scale GDFB is useful for designing a pilot-scale reactor for future applications. The average particle velocities (U_P) (y) as a function of the superficial gas velocity (U_G) (x) of the three types of particles are listed in *Table 3.2*. As the particle density increases, the slopes of these lines increase. Since the net buoyancy force of particles with a higher density is smaller than that of lighter particles, the net acceleration acting on heavier particles is higher. Thus, for a given superficial gas velocity (U_G), the average particle velocity (U_P) is higher for particles with a higher density.

Table 3.2 Linear equations for predicting the average particle velocity (y) based on the superficial gas velocity (x)

Particle Type	Density ρ_P (kg/m^3)	Linear Equation
A	904	$y = 7.64x + 2.63$
B	930	$y = 8.68x + 7.84$
C	950	$y = 9.17x + 7.78$



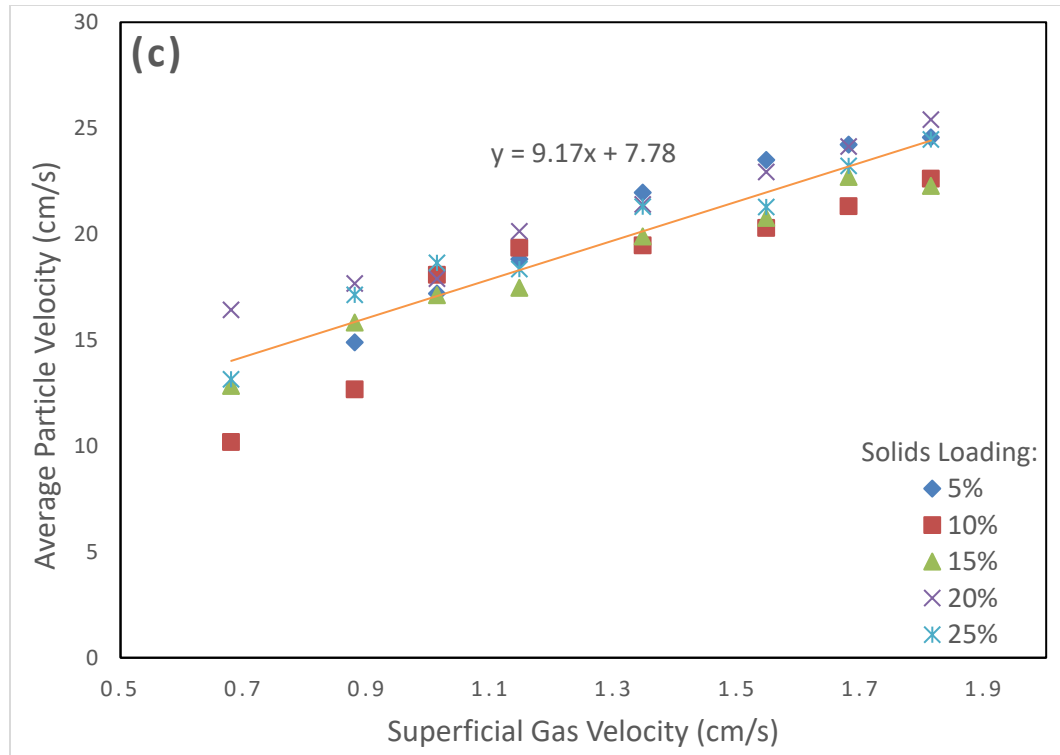


Figure 3.9 Average particle velocity (U_p) versus the superficial gas velocity (U_G) at different solids loadings for particles with a density of (a) 904 kg/m^3 , (b) 930 kg/m^3 , and (c) 950 kg/m^3 in the main system.

To visualize the effect of particle properties, the 5% and 10% solids loading were selected and the average particle velocity (U_p) is plotted against the superficial gas velocity (U_G) for three types of particles in Figure 3.10. The average particle velocity (U_p) of particles with a density of 904 kg/m^3 is larger than that of particles with a density of 930 kg/m^3 . Since the diameters of both particles are the same, it can be concluded that a higher particle density results in a higher average particle velocity (U_p). Under the same gas flowrate, the drag force acting on heavier particles is larger than that on lighter particles. Therefore, particles with a larger density would have a higher average particle velocity (U_p).

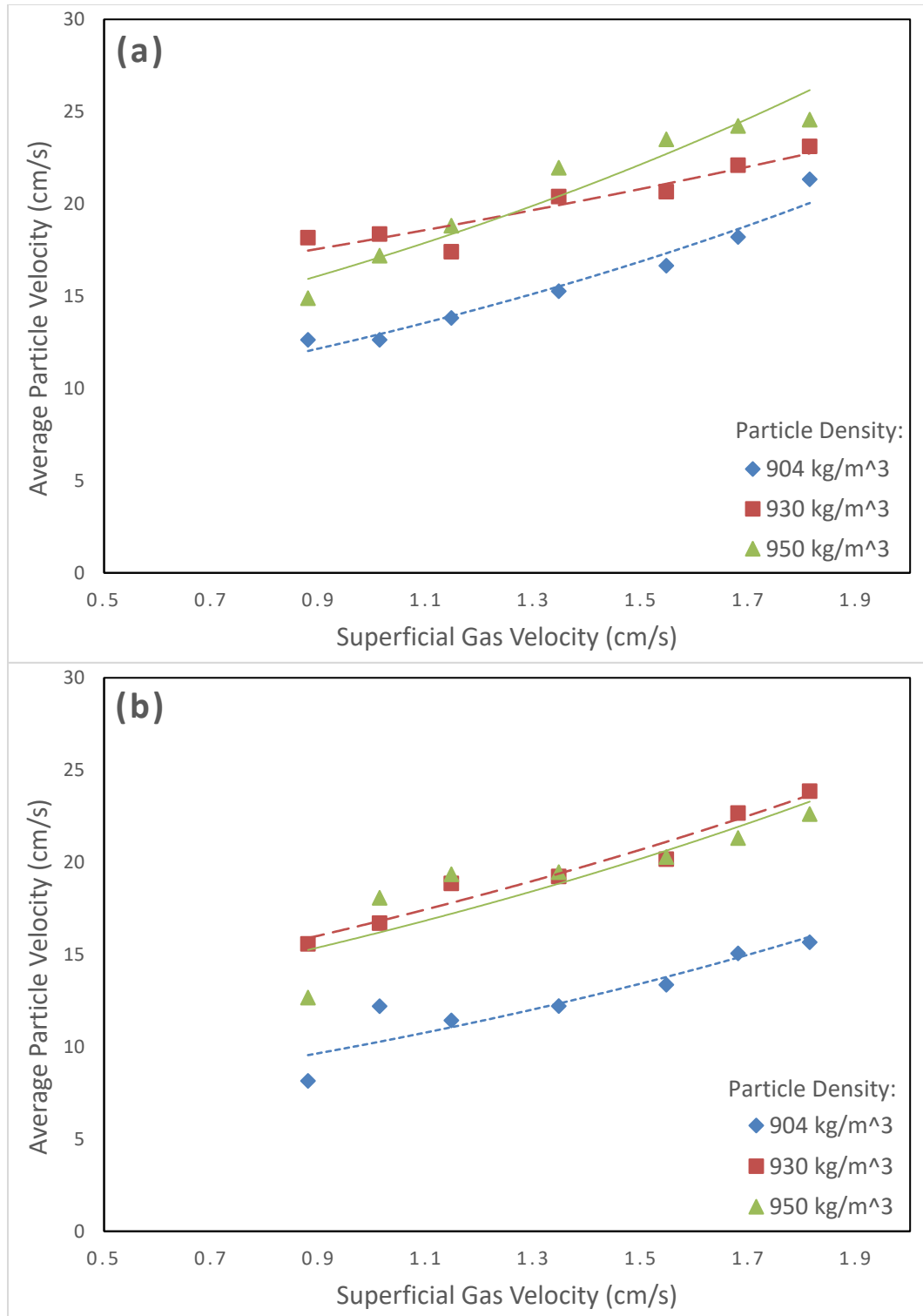


Figure 3.10 Average particle velocity (U_p) versus superficial gas velocity (U_G) for three types of particles at (a) 5% solids loading and (b) 10% solids loading in the main system.

3.4 The Alternative System

3.4.1 The Fluidization Regimes

In the alternative system, a baffle with mesh was installed in the GDFB and five flow regimes were determined as the gas flowrate increases (*Figure 3.11*). At a low gas flowrate, particles stay at the top of the downer as a packed bed. The onset of fluidization is obtained when the initial fluidization velocity (U_{if}) is fulfilled. As the gas velocity increases slightly, some particles are fluidized while the others still remain in the packed bed, which is the semi-fluidized bed. When the gas velocity is beyond the uniform fluidization velocity (U_{uf}), particles form the fully-fluidized bed and the packed bed does not exist. As the gas velocity further increases, the upper boundary of the bed moves away from the water level and the entire fluidized bed is carried downward. This state is defined as the shifted bed and is unique in the meshed-baffle system. Eventually, the conventional fluidized bed is transformed into the circulating bed when the transition velocity (U_{tr}) is reached.

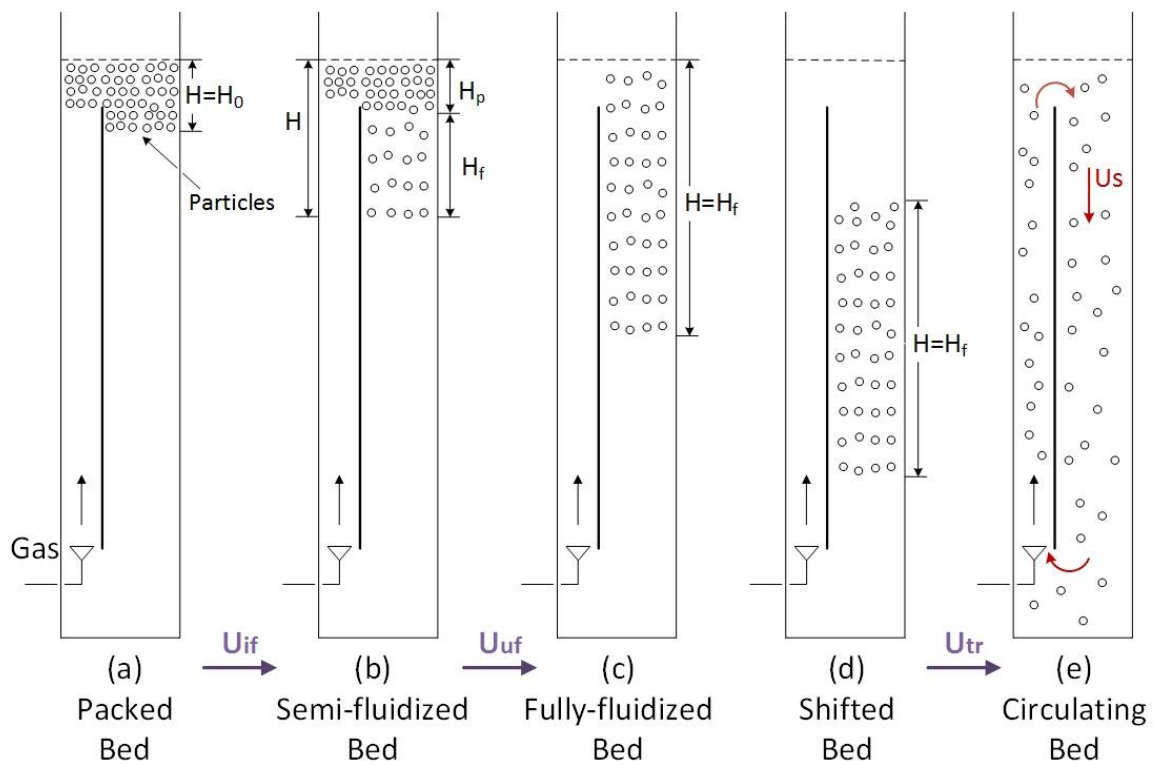


Figure 3.11 The fluidization regimes of the GDFB in the alternative system

3.4.2 Transition Velocity

The transition velocity (U_{tr}) versus solids loading for the systems with a solid baffle and a meshed baffle, respectively (*Figure 3.12*). For both systems, the solids loading does not have a significant effect on the transition velocity (U_{tr}). When all the particles are fluidized, the forces acting on each particle can be considered identical throughout the bed. Thus, each particle requires the same drag force to achieve the circulation. On the other hand, the transition velocity (U_{tr}) in a meshed-baffle system is higher than that in a solid-baffle system. One possible reason is that the mesh allows some of the downward liquid flow to pass through the baffle from the downer to the riser as the pressure in the riser is lower. For the same gas flowrate, the liquid flowrate reaching the bottom of the downer is reduced, which results in a smaller driving force for particles to cross the baffle. Hence, compared to the solid-baffle system, a reactor with a meshed baffle requires a higher gas flowrate to achieve the required liquid velocity for circulation in the downer.

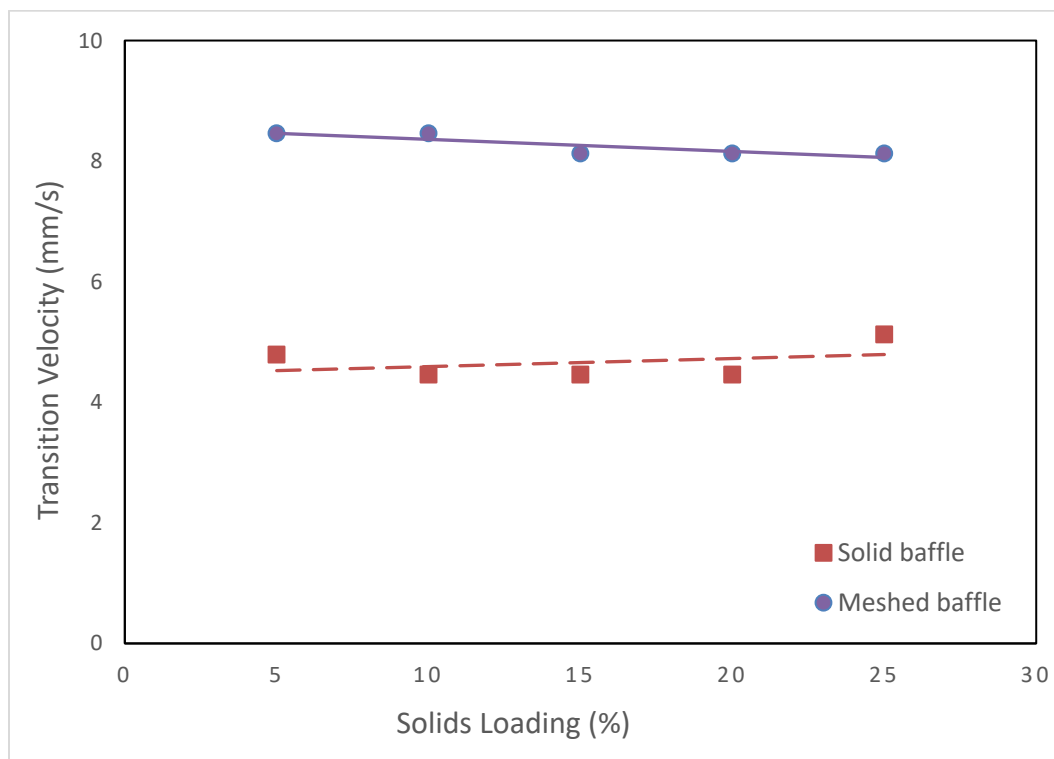


Figure 3.12 Transition velocity (U_{tr}) versus solids loading for particles with 930 kg/m^3 in the main system with a solid baffle and in the alternative system with a meshed baffle.

3.4.3 Average Particle Velocity

The plot of the average particle velocity (U_P) versus the superficial gas velocity (U_G) at different solids loadings is shown in *Figure 3.13*. The increase of the superficial gas velocity (U_G) causes an increase of the average particle velocity (U_P), which is the same trend found in the solid-baffle system. Increasing the liquid flowrate increases the drag force acting on the particles and thus the average velocity of particles circulating in the reactor. Moreover, for all the solids loadings, the maximum deviation of data points from the average line is 14%. Thus, the solids loading does not affect the average particle velocity (U_P) in a meshed-baffle system. Similarly, the average particle velocity (U_P) (y) has a linear relationship with the superficial gas velocity (U_G) (x) and the equation is $y = 7.67x + 21.96$.

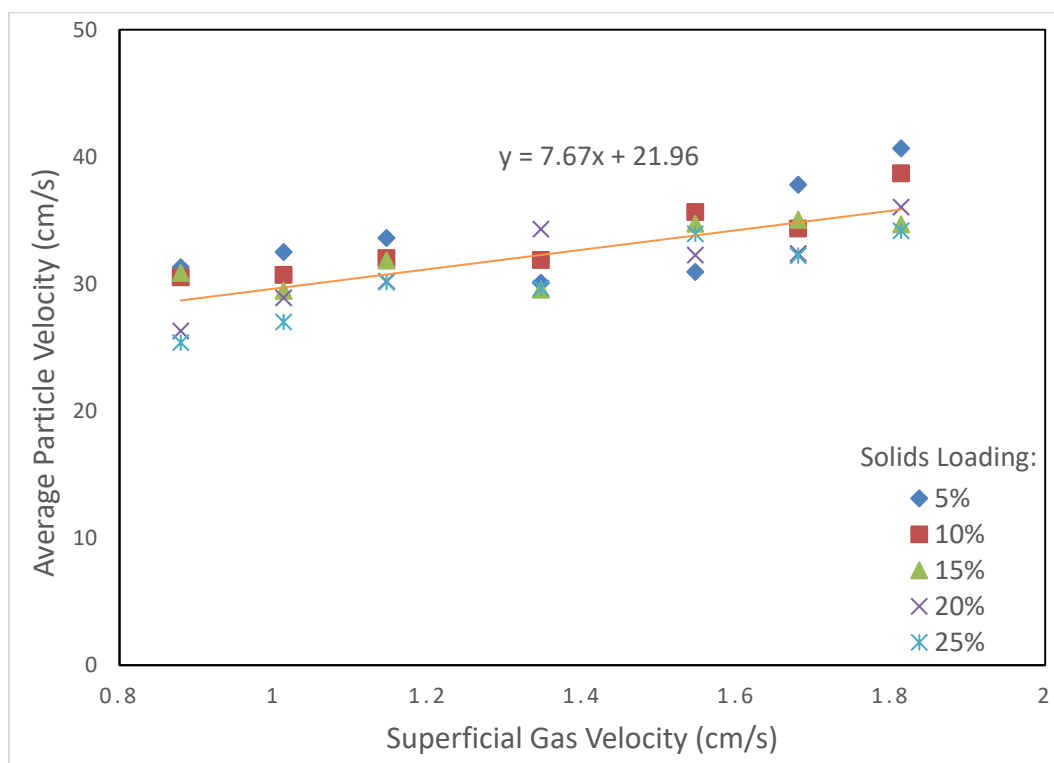


Figure 3.13 Average particle velocity (U_P) versus superficial gas velocity (U_G) at different solids loadings for particles with 930 kg/m^3 in the alternative system.

Furthermore, the average particle velocity (U_P) versus the superficial gas velocity (U_G) is plotted for both systems with a meshed baffle and a solid baffle at 15% solids loading (*Figure 3.14*). It is obvious that the higher average particle velocity (U_P) exists in the meshed-baffle system rather than in the solid-baffle system. Considering the downer alone, the movement of particles is driven by a single stream of liquid from the top of the riser in the solid-baffle system. In contrast, the actual liquid flow in the meshed-baffle system could be the combination of the liquid from the top of the riser and the liquid crossing the mesh. Therefore, for the same superficial gas velocity (U_G), the total liquid flowrate in the meshed-baffle system may be higher than that in the solid-baffle system. Particles experience a larger drag force when the liquid velocity is higher.

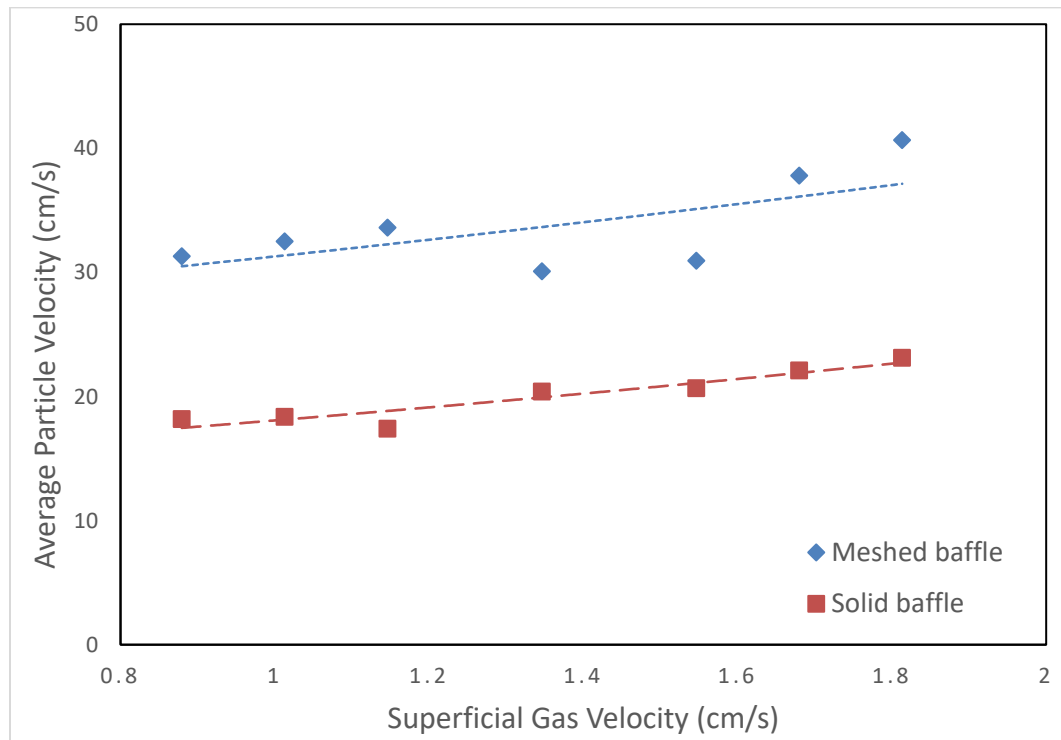


Figure 3.14 Average particle velocity (U_P) versus superficial gas velocity (U_G) at 15% solids loading for particles with 930 kg/m^3 in the alternative system and the main system.

3.5 Conclusions

The transition velocity (U_{tr}) from the conventional regime to the circulating regime and average particle velocity (U_p) in the downer of the gas-driven inverse liquid-solid fluidized bed (GDFB) were determined experimentally in this study. In the GDFB with either a solid baffle or a meshed baffle, the average particle velocity (U_p) increases linearly with the increase of the superficial gas velocities (U_G). The transition velocity (U_{tr}) and the average particle velocity (U_p) do not depend on the solids loading but are inversely proportional to the particle density. However, both the transition velocity (U_{tr}) and the average particle velocity (U_p) are higher in the meshed-baffle system than that in a solid-baffle system. Therefore, a solid baffle is preferable regarding the stable operation and energy efficiency. Since the lab-scale circulating fluidization was achieved by low gas flowrates, the GDFB can be considered as an excellent candidate for biochemical processes requiring low energy consumption. The basic hydrodynamics studied in this paper may contribute to exploring the future applications of this reactor or designing the pilot-scale GDFB.

Nomenclature

Ar	Archimedes number defined by $d_p^3 g (\rho_p - \rho_L) \rho_L / \mu_L^2$
C_D	Drag coefficient
d_p	Particle diameter (mm)
g	Gravitational acceleration on earth (m/s^2)
ID	Inner diameter of the column (cm)
L_e	Effective distance between the two channels of OFP (mm)
n	Number of moles of gas molecules (mol)
P	Absolute pressure (Pa)
R	Gas constant (J/mol.K)
T	Temperature (K)
T_{AB}	Time lag between signals received by two channels of OFP (s)
U_G	Superficial gas velocity (cm/s)
U_{if}	Initial fluidization velocity (cm/s)
U_p	Average particle velocity (cm/s)
U_t	Terminal velocity of particles (cm/s)
U_{tr}	Transition velocity (cm/s)
U_{uf}	Uniform fluidization velocity (cm/s)
V	Volume of gas (m^3)

Abbreviations

GDFB	Gas-driven inverse liquid-solid fluidized bed
IFB	Inverse fluidized bed
LSCFB	Liquid-solid circulating fluidized bed
OFP	Optical fiber probe
PE	Polyethylene
PP	Polypropylene

Greek letters

μ_L	Liquid viscosity being 1.002×10^{-3} Pa.s at 20°C (Pa.s)
ρ_L	Liquid density (kg/m ³)
ρ_P	Particle density (kg/m ³)
ϕ	Particle sphericity
ϕ_{AB}	Cross corelation

Subscripts

G	Gas
if	Initial fluidization
L	Liquid
P	Particle
tr	Transition
uf	Uniform fluidization

References

- Chowdhury, N., Zhu, J., Nakhla, G., Patel, A., & Islam, M. (2009). A Novel Liquid-Solid Circulating Fluidized-Bed Bioreactor for Biological Nutrient Removal from Municipal Wastewater. *Chemical Engineering and Technology*, 32(3), 364–372. <http://doi.org/10.1002/ceat.200800564>
- Fan, L., Muroyama, K., & Chern, S.-H. (1982). Hydrodynamic Characteristics of Inverse Fluidization in Liquid-Solid and Gas-Liquid-Solid Systems. *The Chemical Engineering Journal*, 24, 143–150.
- Huang, J., & Zhu, J.-X. (Jesse). (2017). *Hydrodynamics in the Gas-Driven Inverse Liquid-Solid Fluidized Bed: Chapter 2*. Western University.
- Karamanev, D. G. (1996). Equations for calculation of the terminal velocity and drag coefficient of solids spheres and gas bubbles. *Chemical Engineering Communications*, 147, 75–84.
- Lan, Q., Zhu, J. (Jesse), Bassi, A. S., Margaritis, A., Zheng, Y., & Rowe, G. E. (2000). Continuous Protein Recovery Using a Liquid-Solid Circulating Fluidized Bed Ion Exchange System: Modelling and Experimental Studies. *The Canadian Journal of Chemical Engineering*, 78, 858–866.
- Liang, W.-G., Zhu, J.-X., Jin, Y., Yu, Z.-Q., Wang, Z.-W., & Zhou, J. (1996). Radial Nonuniformity of Flow Structure in a Liquid-Solid Circulating Fluidized Bed. *Chemical Engineering Science*, 51(10), 2001–2010.
- Liang, W., Zhang, S., Zhu, J.-X., Jin, Y., Yu, Z., & Wang, Z. (1997). Flow characteristics of the liquid-solid circulating fluidized bed. *Powder Technology*, 90, 95–102.
- Nikolov, L., & Karamanev, D. (1987). Experimental Study of the Inverse Fluidized Bed Biofilm Reactor. *The Canadian Journal of Chemical Engineering*, 65(April 1987), 214–217.
- Patel, M., Bassi, A. S., Zhu, J. J.-X., & Gomaa, H. (2008). Investigation of a Dual-

- Particle Liquid-Solid Circulating Fluidized Bed Bioreactor for Extractive Fermentation of Lactic Acid. *Biotechnology Progress*, 24, 821–831.
<http://doi.org/10.1021/bp.6>
- Renganathan, T., & Krishnaiah, K. (2003). Prediction of Minimum Fluidization Velocity in Two and Three Phase Inverse Fluidized Beds. *The Canadian Journal of Chemical Engineering*, 81(August), 853–860.
- Renganathan, T., & Krishnaiah, K. (2004). Liquid phase mixing in 2-phase liquid-solid inverse fluidized bed. *Chemical Engineering Journal*, 98(August 2003), 213–218.
<http://doi.org/10.1016/j.cej.2003.08.001>
- Sabarunisha Begum, S., & Radha, K. V. (2014). Hydrodynamic behavior of inverse fluidized bed biofilm reactor for phenol biodegradation using *Pseudomonas fluorescens*. *Korean Journal of Chemical Engineering*, 31(3), 436–445.
<http://doi.org/10.1007/s11814-013-0260-z>
- Sang, L. (2013). *Particle Fluidization in Upward and Inverse Liquid-Solid Circulating Fluidized Bed*.
- Trivedi, U., Bassi, A., & Zhu, J.-X. (Jesse). (2006). Continuous enzymatic polymerization of phenol in a liquid-solid circulating fluidized bed. *Powder Technology*, 169, 61–70. <http://doi.org/10.1016/j.powtec.2006.08.001>
- Ulaganathan, N., & Krishnaiah, K. (1996). Hydrodynamic characteristics of two-phase inverse fluidized bed. *Bioprocess Engineering*, 15, 159–164.
- Vijaya Lakshmi, A. C., Balamurugan, M., Sivakumar, M., Newton Samuel, T., & Velan, M. (2000). Minimum fluidization velocity and friction factor in a liquid-solid inverse fluidized bed reactor. *Bioprocess Engineering*, 22, 461–466.
- Zheng, Y., & Zhu, J.-X. (Jesse). (2001). The onset velocity of a liquid-solid circulating fluidized bed. *Powder Technology*, 114, 244–251.
- Zheng, Y., Zhu, J.-X. (Jesse), Wen, J., Martin, S. A., Bassi, A. S., & Margaritis, A.

(1999). The Axial Hydrodynamic Behavior in a Liquid-Solid Circulating Fluidized Bed. *The Canadian Journal of Chemical Engineering*, 77, 284–290.

Zhu, J.-X. (Jesse), Zheng, Y., Karamanev, D. G., & Bassi, A. S. (2000). (Gas-) Liquid-Solid Circulating Fluidized Beds and their Potential Applications to Bioreactor Engineering. *The Canadian Journal of Chemical Engineering*, 78(February), 82–94.

Chapter 4

4 Conclusions and Recommendations

4.1 Conclusions

In this research, a new type of reactor named Gas-Driven Inverse Liquid-Solid Fluidized Bed (GDFB) was constructed and the hydrodynamic characteristics were studied. The fluidization regimes in the GDFB have been identified and the effects of superficial gas velocity (U_G), solids loading, and particle density on the critical velocities, bed expansion, and average particle velocity (U_p) were also discussed. To compare the effect of baffle structure on the hydrodynamics, the majority of the experiments were conducted using a solid baffle while the other set of experiments were done in the system with a meshed baffle for particles with 930 kg/m^3 .

In the main system, the four fluidization regimes are the packed bed, semi-fluidized bed, fully-fluidized bed, and circulating bed. Compared to a baffle with mesh, a solid baffle is preferable for stable inverse fluidization in the GDFB under the conventional regime and is also more energy efficient. In such a system, the superficial gas velocities (U_G) required for the onset of fluidization, the uniform fluidization, and the onset of circulation are inversely proportional to the particle density. Furthermore, the increase of solids loading led to the increase of the initial fluidization velocity (U_{if}) and the uniform fluidization velocity (U_{uf}). As the superficial gas velocity (U_G) increased, the fluidized bed height (H_f) increased and the packed bed height (H_p) decreased. The speed of bed expansion was higher for light particles with a higher density and for a smaller solids loading. Also, the average particle velocity (U_p) under the circulating regime increased with increasing gas flowrate and is in inverse proportion to the particle density. Solids loading did not demonstrate a significant impact on the average particle velocity (U_p).

In a meshed-baffle system, except for the same four regimes as the solid-baffle system, the shifted bed was found to lay between the fully-fluidized bed and circulating bed. The relationships between the particle density or the solids loading and the hydrodynamics are similar in both the solid-baffle system and the meshed-baffle system. One exception is

that the initial fluidization velocity (U_{if}) in a meshed-baffle system did not change with the solids loading. Another difference is that the bed expansion in the mesh-baffle system did not follow a constant increase or decrease. Therefore, depending on the purpose of each chemical process, a solid baffle or a meshed baffle can be selected to be installed in the GDFB.

4.2 Recommendations

In this research, only three types of particles were used and they have different material, density, size, or shape. It is necessary to adopt particles sharing common properties for accurate comparison of the effects of each property. Moreover, to confirm the fluidization regimes, the pressure drop profile and uniformity of particles distribution should be investigated. In addition, the hydrodynamic characteristics determined from experiments should be verified by that from model prediction. Bubble behaviors, actual liquid velocity, and mass transfer rates may be needed for many chemical reactions. Furthermore, the ratio of the riser and downer can be varied to investigate the optimal condition for fluidization. In brief, more work is essential to completely understand the hydrodynamics and potential applications of this novel GDFB.

Appendices

Appendix A. Examples of error analysis

To make sure the accuracy of experimental results, a few sets of data were randomly selected to perform the error analysis. Examples of error bars of the initial fluidization velocity (U_{if}) for particles with a density of 930 kg/m^3 in a solid-baffle system and that in a meshed-baffle system were shown in *Figure. A*. This experiment was repeated for five times.

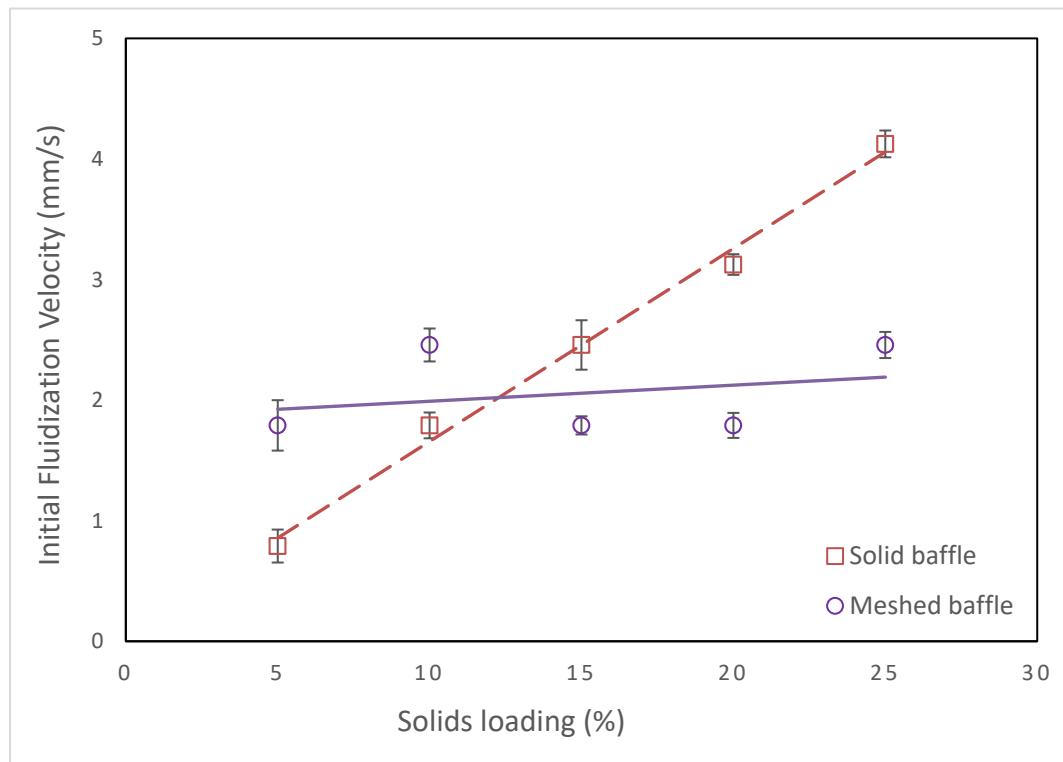


Figure. A Initial fluidization velocity (U_{if}) versus solids loading with error bars for particles with a density of 930 kg/m^3 in the main system and in the alternative system.

The bed expansion ratio (H/H_0) with error bars for particles with 904 kg/m^3 at 5% solids loading in the main system is shown in *Figure. B*. This measurement of bed heights was repeated for five times. In addition, *Figure. C* displays an example of error bars of the average particle velocity (U_p) for particles with a density of 930 kg/m^3 in a solid-baffle system at 15% solids loading, according to three sets of data collected by the OFP.

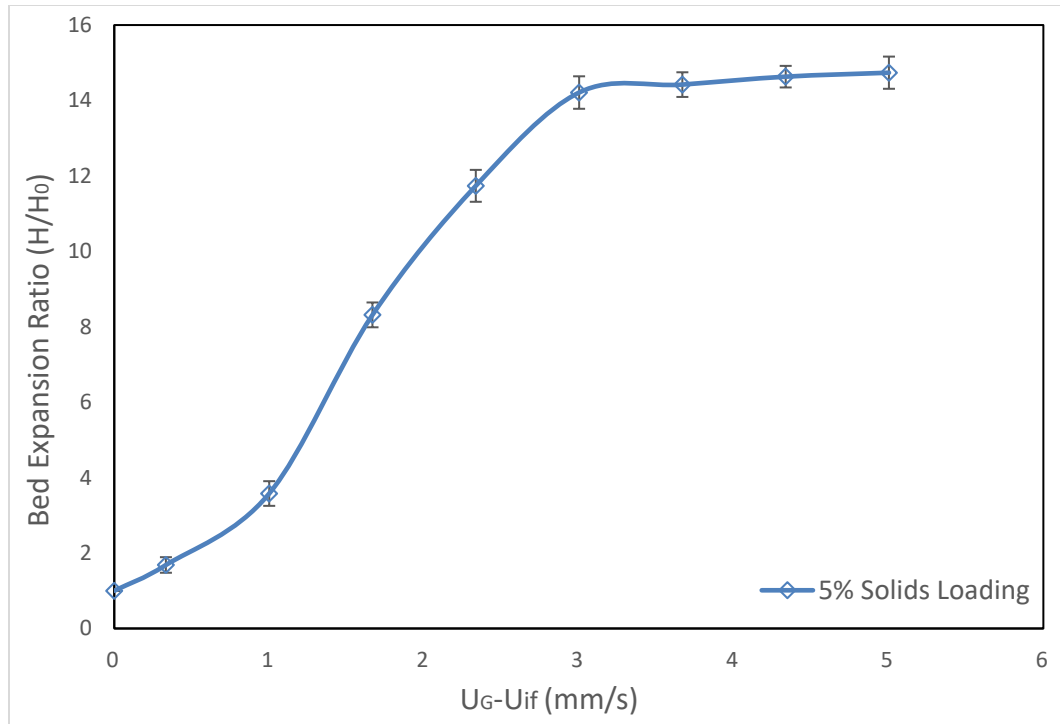


Figure. B Bed expansion ratio (H/H_0) with error bars for particles with 904 kg/m^3 at 5% solids loading in the main system.

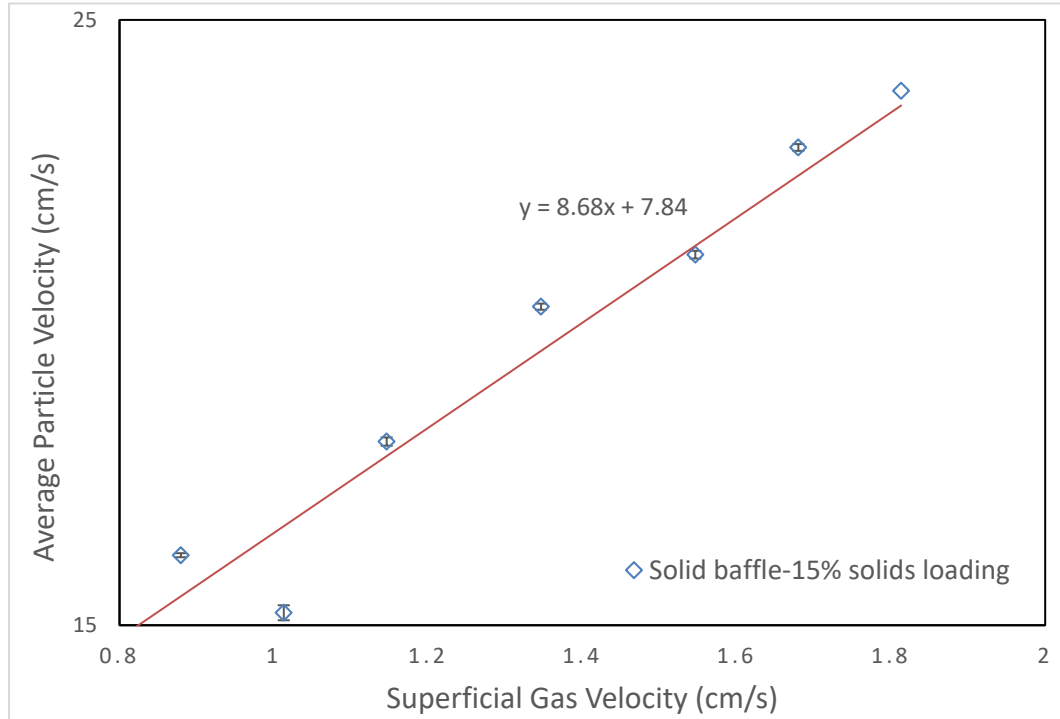


Figure. C Average particle velocity (U_P) versus superficial gas velocity (U_G) with error bars for particles with a density of 930 kg/m^3 at 15% solids loading in the main system.

Appendix B1. Initial fluidization velocity, uniform fluidization velocity, and transition velocity

Baffle	Particle Density (kg/m³)	Solids Loading	5%	10%	15%	20%	25%
Solid	904	Initial fluidization velocity (mm/s)	1.79	2.46	3.12	4.79	5.79
	930		0.79	1.79	2.46	3.12	4.13
	950		1.70	2.12	2.60	3.46	3.79
Meshed	930		1.79	2.46	1.79	1.79	2.46

Baffle	Particle Density (kg/m³)	Solids Loading	5%	10%	15%	20%	25%
Solid	904	Uniform fluidization velocity (mm/s)	4.13	6.13	6.46	7.13	7.46
	930		3.12	3.79	4.46	4.46	5.13
	950		3.46	4.79	4.46	4.79	4.79
Meshed	930		3.12	4.13	4.79	4.79	5.46

Baffle	Particle Density (kg/m³)	Solids Loading	5%	10%	15%	20%	25%
Solid	904	Transition velocity (mm/s)	7.46	6.79	6.79	7.13	7.46
	930		4.79	4.46	4.46	4.46	5.13
	950		6.13	6.13	4.79	4.79	4.79
Meshed	930		8.46	8.46	8.13	8.13	8.13

Appendix B2. Average particle velocity

Particles with a density of 904 kg/m³ in the main system

Solids Loading	5%	10%	15%	20%	25%
U_G (cm/s)	Average particle velocity U_P (cm/s)				
0.88	12.63	8.15	8.10	7.24	7.87
1.01	12.63	12.20	11.27	9.86	11.97
1.15	13.82	11.43	8.61	9.80	11.32
1.35	15.26	12.21	11.53	12.80	10.01
1.55	16.65	13.36	14.09	12.06	16.02
1.68	18.21	15.06	16.09	16.56	13.70
1.81	21.33	15.67	14.65	14.64	15.28

Particles with a density of 930 kg/m³ in the main system

Solids Loading	5%	10%	15%	20%	25%
U_G (cm/s)	Average particle velocity U_P (cm/s)				
0.68	15.14	12.74	11.97	11.32	14.27
0.88	18.17	15.58	16.16	16.00	14.64
1.01	18.36	16.70	15.21	15.50	17.35
1.15	17.40	18.86	18.03	19.07	16.68
1.35	20.40	19.24	20.26	20.62	18.53
1.55	20.66	20.17	21.12	21.01	21.40
1.68	22.09	22.67	22.89	22.34	22.04
1.81	23.12	23.86	23.83	23.67	23.28

Particles with a density of 950 kg/m³ in the main system

Solids Loading	5%	10%	15%	20%	25%
U_G (cm/s)	Average particle velocity U_P (cm/s)				
0.68	13.22	10.18	12.83	16.42	13.14
0.88	14.89	12.67	15.83	17.67	17.13
1.01	17.20	18.08	17.12	17.90	18.65
1.15	18.82	19.36	17.47	20.13	18.35
1.35	21.96	19.47	19.89	21.40	21.30
1.55	23.50	20.29	20.76	22.93	21.28
1.68	24.22	21.32	22.70	24.13	23.22
1.81	24.56	22.62	22.28	25.40	24.47

Particles with a density of 930 kg/m³ in the alternative system

Solids Loading	5%	10%	15%	20%	25%
U_G (cm/s)	Average particle velocity U_P (cm/s)				
0.88	31.31	30.51	30.87	26.29	25.38
1.01	32.51	30.71	29.46	28.90	27.01
1.15	33.61	32.02	31.83	30.22	30.14
1.35	30.08	31.87	29.54	34.30	29.66
1.55	30.94	35.66	34.73	32.27	33.94
1.68	37.80	34.35	35.05	32.38	32.23
1.81	40.66	38.70	34.68	36.04	34.17

Appendix C. Rotameter calibration

The air rotameter was calibrated by a gas meter under the atmospheric pressure. *Figure. D* shows the calibration curve used to determine the actual gas flowrate from the readings on the rotameter.

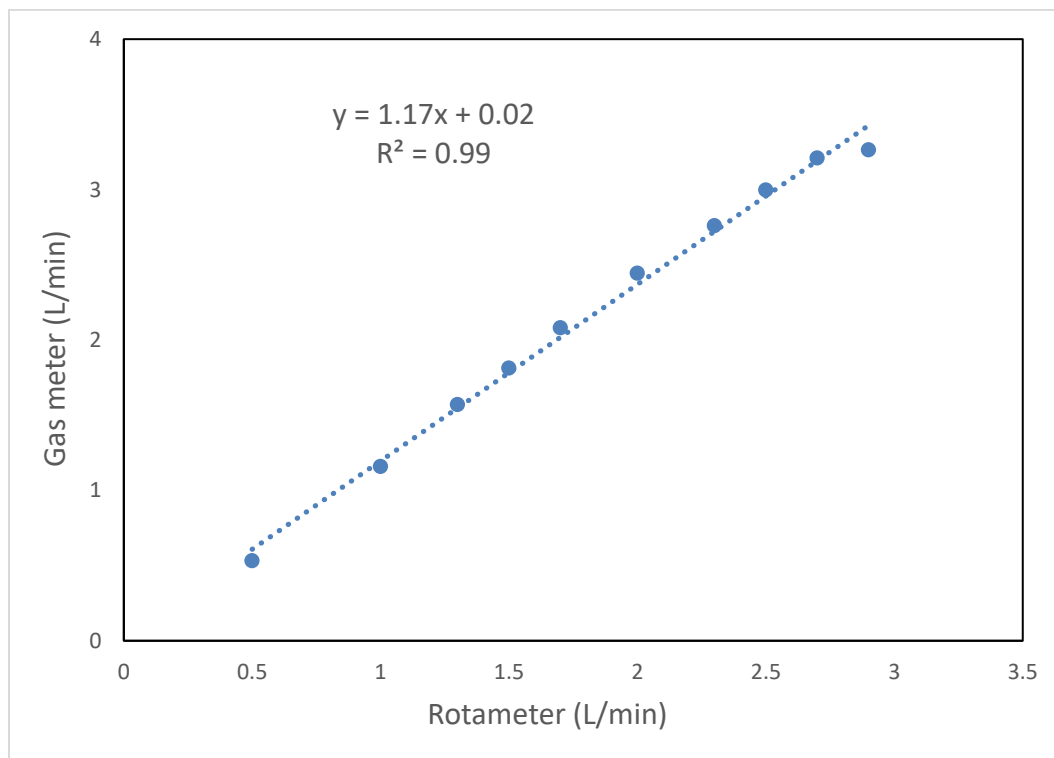


Figure. D Rotameter calibration curve

Curriculum Vitae

Name: Jiaqi Huang

Post-secondary Education and Degrees: Department of Chemical and Biochemical Engineering
Western University
London, Ontario, Canada
2012-2016 B.E.Sc.
2016-2017 M.E.Sc.

Honors and Awards: Dean's Honor List
Western University
2013, 2015

Related Work Experience Teaching Assistant
Research Assistant
Western University
2016-2017